Quaternary Science Reviews 248 (2020) 106546

Contents lists available at ScienceDirect

Quaternary Science Reviews

journal homepage: www.elsevier.com/locate/quascirev

Droughts, flooding events, and shifts in water sources and seasonality characterize last interglacial Levant climate

Yael Kiro [a, b, *], Steven L. Goldstein [a, c], Yochanan Kushnir [a], Jennifer M. Olson [a, c], Louise Bolge [a], Boaz Lazar [d], Mordechai Stein [d, e]

[a] Lamont-Doherty Earth Observatory of Columbia University, 61 Route 9W, Palisades, NY, 10964, USA
[b] Department of Earth and Planetary Sciences, The Weizmann Institute of Science, 234 Herzl St., Rehovot, 7610001, Israel
[c] Department of Earth and Environmental Sciences, Columbia University, 61 Route 9W, Psaalides, NY, 10964, USA
[d] Institute of Earth Sciences, The Hebrew University, Givat Ram, Jerusalem, 91904, Israel
[e] Geological Survey of Israel, 32 Yesha'yahu Leibowitz St., Jerusalem, 9692100, Israel

ARTICLE INFO

Article history:
Received 26 August 2019
Received in revised form
8 August 2020
Accepted 12 August 2020
Available online 16 September 2020

ABSTRACT

Modern observations document increased drought frequency together with more intense precipitation and flooding in the world's semi-arid and arid regions as a consequence of the warming climate. Climate models predict that such conditions will intensify in the future, impacting millions of people. Paleoclimate studies can complement the short modern observational record and model projections by documenting climate changes in the past. Here we report major shifts in the geographic sources, intensity, and seasonality of Eastern Mediterranean precipitation during the unusually warm last interglacial period Marine Isotope Stage (MIS) 5e, reflecting global shifts in the rain and desert belts, based on $^{234}U/^{238}U$-ratios in mineral precipitates in the Dead Sea, combined with evidence from climate model simulations.

In the Dead Sea catchment $^{234}U/^{238}U$ ratios are indicators of water sources, where the Jordan River (flowing from the north) and the western catchments show high activity ratios between ~1.5–1.7, and the eastern and southern catchments and flash floods (in the south-west, south and east) show lower ratios of 1.0–1.2. In Dead Sea water and precipitated minerals, $^{234}U/^{238}U$ is nearly always ~1.45–1.55 during both glacials and interglacials. However, during the last interglacial MIS 5e insolation peak (~127–122 ka) its value decreased to 1.2–1.3, and then to ~1.0 towards its end (~122–116 ka). During the insolation peak, the U-isotope data, combined with climate model runs forced with period orbital and greenhouse gas concentrations, indicate that rainfall associated with the African Summer Monsoon in the Dead Sea catchment accounted for ~50% of the total annual rainfall, in stark contrast to present-day dry summers. The geochemical evidence indicates that following the insolation peak the region experienced an extremely dry period (although punctuated with wetter intervals), signifying expansion of the desert belt, similar to predicted effects of anthropogenic warming. This drying is partly supported by climate model runs forced with the appropriate changes in orbital parameters. The extreme drying during late MIS 5e between ~122–116 ka reflected a major weakening of Mediterranean storm systems, resulting in a major decline of the Jordan River flow (indicated by the low $^{234}U/^{238}U$ ratios in the Dead Sea) and a relative increase in precipitation associated with the African Monsoon, shifting towards autumn. The Jordan River flow is estimated to be ~10% of the present-day (pre-1964, prior to major diversion of the Jordan River and its sources for human use). Such changes, if they occur in the future, have serious implications for future water availability in the politically sensitive Middle East.

1. Introduction

Semi-arid subtropical regions near desert belts are particularly sensitive to global climate changes. Predicted effects of future warming from modern weather trends and climate models (Collins

* Corresponding author. Department of Earth and Planetary Sciences, The Weizmann Institute of Science, 234 Herzl St., Rehovot, 7610001 Israel.
E-mail address: yael.kiro@weizmann.ac.il (Y. Kiro).

https://doi.org/10.1016/j.quascirev.2020.106546
0277-3791/

et al., 2013; Held and Soden, 2006) include increased frequency of droughts and expansion of desert belts, accompanied by more frequent intense rainfall events resulting in flooding (Donat et al., 2019). Paleoclimate studies of previous warm periods provide independent information of what actually happened in the past, which helps to validate such short- and long-term observational and model-based predictions, whose reliability is limited by the uncertainties in the models and the complexity of the climate system.

As a drought-sensitive region with a large population and a scarcity of fresh water (e.g. Kaniewski et al., 2012), the Eastern Mediterranean-Levant (comprising present-day Israel, Jordan, Lebanon, Palestine, Syria) is among the regions on Earth expected to be strongly affected by increased global warming (Kelley et al., 2012, 2015). Climate models predict, and observations show, a drying trend occurring around the Mediterranean during the winter wet season, reflecting the effects of increased greenhouse gases (Kelley et al., 2012). Present-day rainfall is mainly associated with wintertime Mediterranean low-pressure synoptic systems, the most common of which is the "Cyprus Low". The paths of these winter storms subject the region to a sharp north-south rainfall gradient with east-west orographic effects (Fig. 1). The current drying trend is accompanied by more intense flooding events in the Levant, as in other semi-arid regions (Alpert, 2002; Molnar, 2001), which are often associated with increased frequency of tropical moisture incursions (de Vries et al., 2013; Neugebauer et al., 2015). An extremely dry period lasting millennia that occurred during latter stages of the last interglacial Marine Isotope Stage (MIS) 5e is recorded in drill cores recovered by the Dead Sea Deep Drilling Project (DSDDP), funded by the International Continental Scientific Drilling Program (ICDP) and national funding agencies, from the deepest basin of the Dead Sea (Fig. 1). The DSDDP cores provide a climate record over the last ~220 ka (Goldstein et al., 2020; Torfstein et al., 2015) that includes an ~87 m long sedimentary section from MIS 5e, providing an unprecedented high-resolution lake record of the MIS 5e climate in the region (Neugebauer et al., 2014; Torfstein et al., 2015).

This study focuses on the implications of uranium isotope ($^{234}U/^{238}U$) variations in the Dead Sea during MIS 5e (~131–116 ka, Shackleton, 1969; Shackleton et al., 2003), as recorded in precipitated minerals (aragonite, gypsum, and halite), for tracing past changes in rainfall patterns in the Eastern Mediterranean-Levant within the Dead Sea catchment (Fig. 1). The DSDDP cores and the $^{234}U/^{238}U$ proxy provide the opportunity to document major changes in the moisture sources through that time interval.

1.1. The last interglacial in the Eastern Mediterranean-Levant

MIS 5e was characterized with higher average global temperatures, sea-level, and CO_2 concentrations compared to the Holocene (Dutton and Lambeck, 2012; Govin et al., 2015; Jouzel et al., 2007; Lüthi et al., 2008). Terrestrial records show that Southern Europe (Brauer et al., 2007) and the Sahara-Arabian desert belt (Nicholson et al., 2020; Osborne et al., 2008; Petit-Maire et al., 2010; Rosenberg et al., 2013) were warmer and wetter than today. Climate models show that peak summer insolation is associated with a northward expansion of the African summer monsoon and a contraction of the desert belt, while minimum summer insolation (maximum winter insolation) is associated with a relative contraction of the monsoon belt (Kutzbach et al., 2020). A recent study, focused on European and Mediterranean climate, highlights the climate variability at that time, with fluctuations between dry and wet intervals around the Mediterranean related to ice melt pulses in Greenland (Tzedakis et al., 2018). The DSDDP record reveals that wet intervals in the Eastern Mediterranean-Levant during MIS 5e (Bar-Matthews, 2014) alternated with extremely dry periods (Kiro et al., 2017), reflecting high seasonality and climate variability during that time (Felis et al., 2004; Otto-Bliesner et al., 2013). The region was relatively wet between ~127–122 ka, during the Northern Hemisphere insolation peak (Bar-Matthews, 2014; Develle et al., 2011; Nehme et al., 2015; Neugebauer et al., 2016), but experienced more aridity both before and especially afterward, which is also projected by climate models for future warming (Kiro et al., 2017).

These climate changes are recorded by the changes in the sedimentary facies in the DSDDP cores (Neugebauer et al., 2014; Torfstein et al., 2009), with alternating mm-thick layers of aragonite and detritus indicating wetter periods, decreasing amounts of aragonite compared to detritus indicating increasing aridity, and the appearance of gypsum and then halite indicating increasing hyper-aridity (i.e. more arid than today, Figs. S1,S2). In detail, the halite sequences deposited throughout MIS 5e, signifying extreme aridity, are punctuated by halite-free intervals, signifying alternating more-arid and more-wet periods during the drought intervals (Kiro et al., 2016; Torfstein et al., 2015). A ~20 m thick halite-free detritus interval (in which part of it is alternating aragonite and detritus) deposited at ~127–122 ka (ages are discussed in Section 2) is evidence for a long 'wetter' interval that coincided with the summer (JJA) tropical insolation maximum (Fig. 2,S1). This wetter interval was also associated with an African wet period, marked by expansion and intensification of the tropical African Monsoon belt, which resulted in high Nile flow that caused anoxic conditions and a major sapropel event (Sapropel 5) signifying anoxia in the Eastern Mediterranean (Rossignol-Strick, 1983). Coeval wetness in and near the Dead Sea watershed is evidenced by speleothem growth and travertine formation in the Negev (Vaks et al., 2010, 2006; Waldmann et al., 2010), which is not occurring today and thus indicates higher rainfall than the present-day in the desert south of the Dead Sea (Fig. 2). Following this halite-free Sapropel 5 interval, the most intense known drought of the late Quaternary in the Levant occurred between ~122–116 ka, evidenced by ~28 m of halite over ~50 m of core length (Kiro et al., 2017).

Interpretations of MIS 5e Levant climate records have concluded both that it was arid (Kiro et al., 2017; Torfstein et al., 2015; Waldmann et al., 2009) and wet (Bar-Matthews, 2014; Bar-Matthews et al., 2003), with moisture from either tropical (Torfstein et al., 2015; Waldmann et al., 2010), Mediterranean (Bar-Matthews, 2014; McGarry et al., 2004) or Atlantic (Bosmans et al., 2020) sources. The drier conditions are reflected in the Dead Sea by low lake levels, increases in Mg concentration in pore waters, and deposition of halite (Kiro et al., 2017; Torfstein et al., 2015; Waldmann et al., 2009). The evidence for wetter conditions is reflected by low $\delta^{18}O$ values in the Soreq Cave speleothems (Bar-Matthews et al., 2003) and the occurrence of travertines (Waldmann et al., 2010) and speleothems (Vaks et al., 2010, 2006) in the Negev desert. As for the sources of moisture, fluid inclusions in Soreq speleothems indicate Mediterranean moisture sources (McGarry et al., 2004), while the occurrence and distribution of speleothems and travertines in the Negev have been interpreted as indicating both Mediterranean (Bar-Matthews, 2014; Vaks et al., 2010) and tropical (Waldmann et al., 2010) sources. A recent ion probe $\delta^{18}O$ study of Soreq speleothems at annual to decadal temporal resolution shows evidence for summer monsoonal precipitation during the peak insolation of MIS 5e (Orland et al., 2019). These opposing interpretations reflect the proxies used and the temporal resolution of the archives. For example, the Soreq cave speleothem record does not necessarily highlight the dry intervals revealed by the DSDDP core. Advantages of the DSDDP cores compared to other Eastern Mediterranean region climate archives include the long core length covering MIS 5e (~87 m) offering high temporal resolution, and the stratigraphic continuity resulting from

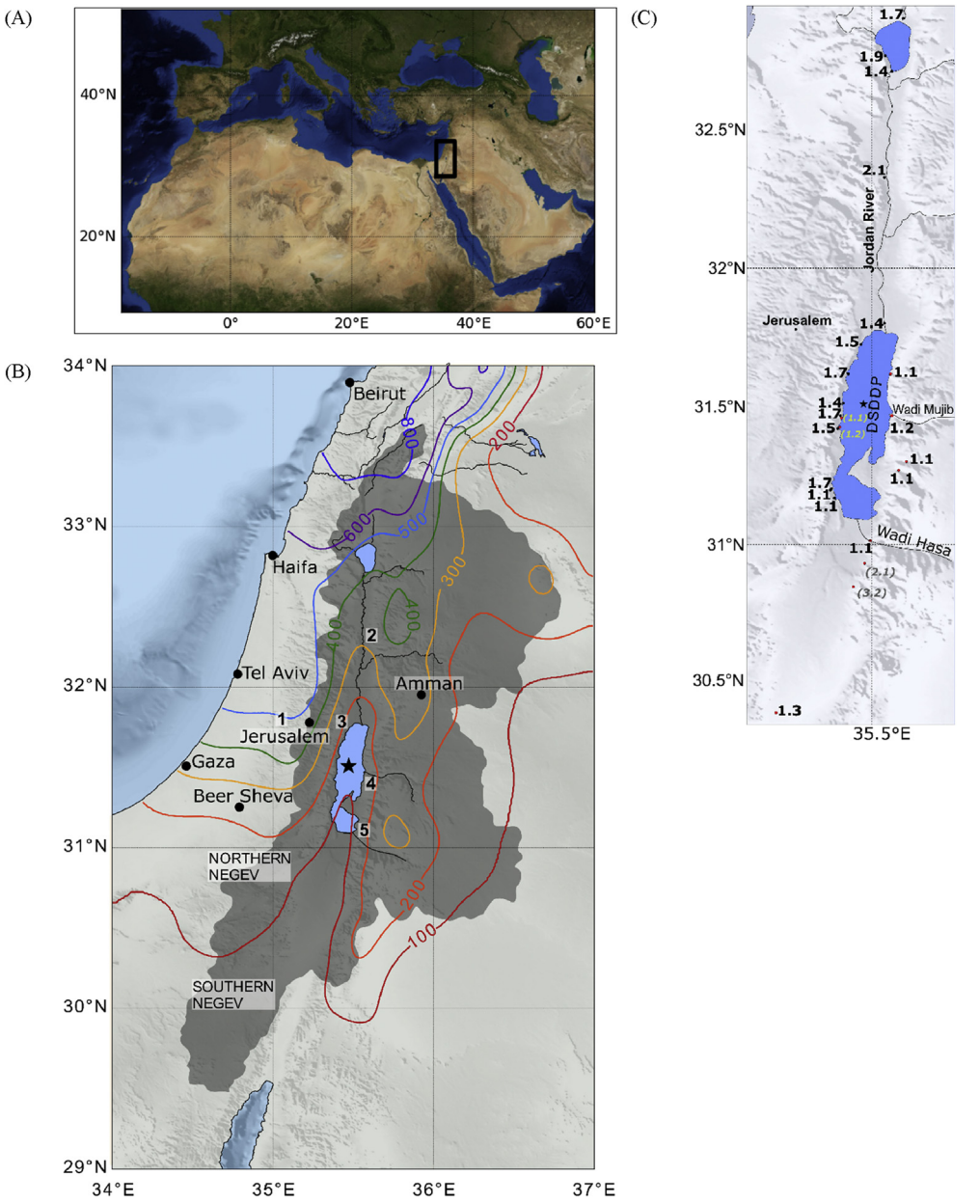

Fig. 1. (A) Map showing the location of the Levant and Dead Sea watershed (rectangle), between the Mediterranean climate zone and the Saharan-Arabian desert belt. (B) Map showing precipitation contours (mm/y) superimposed on a map of the Dead Sea watershed, along with the locations of the DSDDP core (star), Soreq Cave (1), and important water sources around the Dead Sea: Jordan River (2), Ein-Feshkha springs (3), Wadi Mujib (4), and Wadi Hasa (5). Precipitation contours are from WorldClim 2 (Fick and Hijmans, 2017). (C) $^{234}U/^{238}U$ activity ratios in the Dead Sea water sources (published (Haase-Schramm et al., 2004) and new data (in red dots) summarized in Table S2). The water main source is the Jordan River with values of ~1.5. Values in parenthesis are in minor streams in Jordan (gray) and in hot brines with very low U (yellow). (For interpretation of the references to colour in this figure legend, the reader is referred to the Web version of this article.)

its location in the deepest part of the Dead Sea. Even when the lake level was the lowest, the salt facies suggest a deep lake (Kiro et al., 2016). The cores record alternating intervals of wetness and dryness occur through the entire MIS 5e record (suggesting that both conclusions may be partly correct), even during the driest periods. This study, using the DSDDP cores and its $^{234}U/^{238}U$ record, aims to reconcile these apparent discrepancies by showing that precipitation was highly variable and that the relative contributions of moisture from northern and southern sources varied throughout MIS 5e.

1.2. The Dead Sea and $^{234}U/^{238}U$ isotope ratios

The Dead Sea is a terminal lake, with an extreme salinity of 340 g/L (Katz and Starinsky, 2008), about 10 times seawater. Its water level marks the lowest surface elevation on the continents, which is now (2020) 434 mbsl (meters below sea level). Its watershed includes the Mediterranean climate zone in the north, with dry summers and wet winters, and the arid Saharan-Arabian desert belt in the south (Fig. 1). The natural lake level varies with changes in water discharge, which in turn varies with rainfall within the watershed (Enzel, 2003). On decadal time scales, observed Levant rainfall records, from Beirut and Damascus in the north to Beer Sheva in the south, display well correlated variations

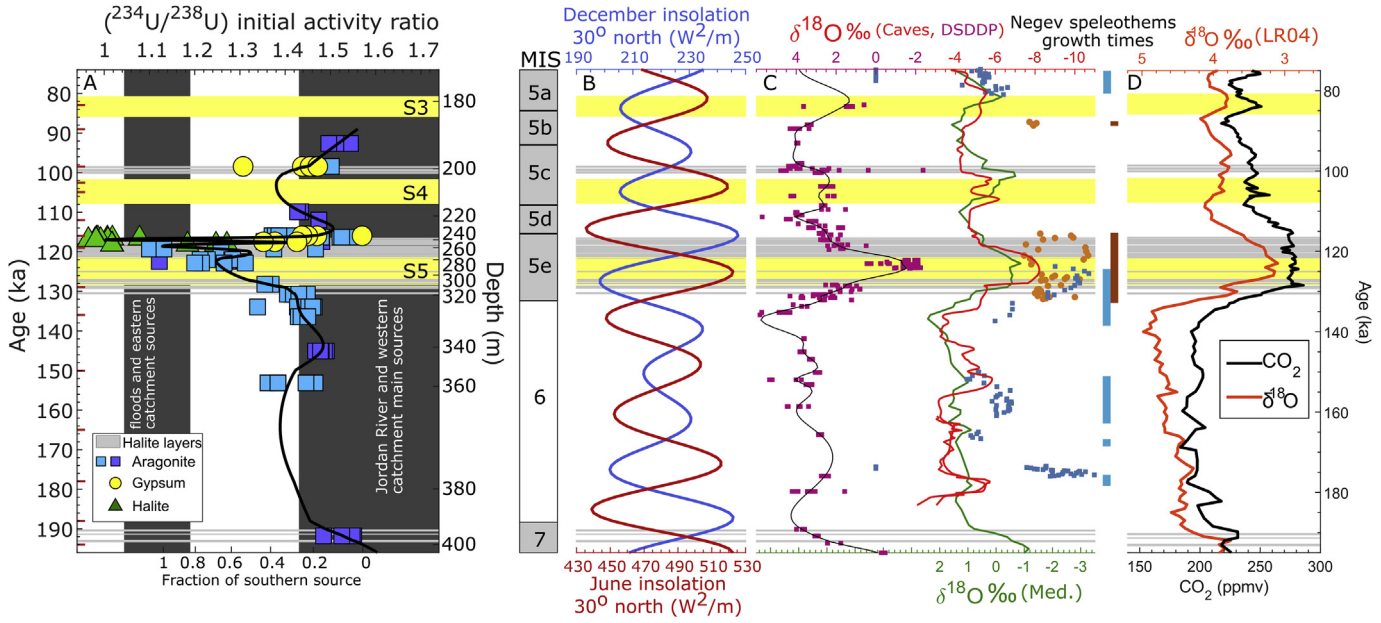

Fig. 2. (A) Initial $^{234}U/^{238}U$ (activity) ratios in authigenic minerals in the DSDDP core versus age (left axis) and depth in the DSDDP core (right axis) showing a major shift during MIS 5e from ~1.4–1.5 (typical for both glacials and interglacials) to near secular equilibrium values, reflecting major changes in Dead Sea water sources from the north and west (Jordan River and Mediterranean-sourced rainfall) to the south and east (ranges of the two regions shown by vertical orange bars). Black line is a spline fit to the data. Dark blue symbols mark aragonite samples from Torfstein et al. (2015), others are from this study. Analytical errors are ±0.01 activity units, about the size of the samples symbol. Ages of Marine Isotope Stages are shown on the right. Anchor ages are marked by the red ticks (Goldstein et al., 2020). (B) Summer (red) and winter (blue) insolation curves at 30°N (Laskar et al., 2004). (C) $\delta^{18}O$ in DSDDP aragonite(2015), the Mediterranean $\delta^{18}O$ stack from G. ruber in cores KC01B, MD84-641, ODP Site 967(Wang et al., 2010), Soreq Cave speleothems (Bar-Matthews et al., 2003; Grant et al., 2012) after smoothing by a Gaussian filter (σ ~100y), northern Negev (Vaks et al., 2006) and southern Negev speleothems (Vaks et al., 2010). The age intervals of Negev speleothem growth are indicated by blue (N. Negev) and brown (S. Negev) bars. (D) Atmospheric CO_2 from Antarctic ice cores (Bereiter et al., 2015), and the LR04 $\delta^{18}O$ oceanic benthic stack (Lisiecki and Raymo, 2005). The DSDDP age model is based on Torfstein et al. (2015) In all frames, gray stripes show the ages/depths of halite deposition, yellow stripes show the intervals of Mediterranean sapropels S5, S4 and S3 (Grant et al., 2016; Rossignol-Strick, 1983). (For interpretation of the references to colour in this figure legend, the reader is referred to the Web version of this article.)

between the stations (Enzel, 2003; Kushnir and Stein, 2010). Principal component analysis of the data shows that 70% of the annual precipitation variance between stations is explained by the first component (Enzel, 2003), reflecting the regional patterns. The main water source is the Jordan River (Fig. 1), which supplied ~1300 Mm^3/y before 1964, when the river was dammed, thus "present-day runoff" in this paper refers to pre-1964. Since then, fresh water has been increasingly diverted for human use. Springs and ephemeral flows contribute ~300 Mm^3/y (Lensky et al., 2005; Salameh and El-Naser, 1999). Moisture for the Jordan River and the western catchments is mainly contributed by Mediterranean winter storm systems, while moisture from southern synoptic systems occurring during fall through spring often cause flash flooding in the Sahara-Arabian desert zone (de Vries et al., 2013; Kahana et al., 2002).

The Dead Sea is mainly fed by groundwater discharging into streams that flow into the lake, including the Jordan River (Lensky et al., 2005; Salameh, 1996; Salameh and Udluft, 1985). The source of U into the lake is mainly the fresh water flowing into it. Its residence time in the Dead Sea is ~300 years (Section 1.3), thus changes can be observed on the scale of centuries, and steady-state is obtained after ~1500 years. Our estimate of the uranium residence time in the Dead Sea of ~300 years is based on ~0.6 ppb U in water sources, the pre-1964 total runoff of 1600 Mm^3/y, ~1.8 ppb U in the lake, and a volume of 150 km^3. Dissolved U is removed from the Dead Sea water by authigenic mineral precipitation, adsorption on particles, and redox effects of Dead Sea water circulation in aquifers (Kiro et al., 2014). Compared with other isotopic provenance tracers, uranium is more soluble than Nd and Pb, and has a shorter residence time in the lake than Sr, making it useful for tracking changes in water resources. Dead Sea lake levels are higher during glacials and lower during interglacials (Neev and Emery, 1967), nevertheless the $^{234}U/^{238}U$ activity ratio of the Dead Sea has remained close to ~1.45–1.55 during the last ~200,000 years through both interglacials and glacials, primarily reflecting the value of the Jordan River (Fig. 2) and the dominance of its input (Haase-Schramm et al., 2004; Torfstein et al., 2013).

1.3. $^{234}U/^{238}U$ systematics

$^{234}U/^{238}U$ ratios are usually greater than 1 (all $^{234}U/^{238}U$ values listed are activities) in groundwaters due to α-recoil during U decay that damages mineral lattice sites, causing the ^{234}U sites to be more susceptible to weathering than ^{238}U (e.g. Porcelli and Swarzenski, 2003), and in waters it may reach values up to ~10. As a consequence, present-day seawater is enriched in ^{234}U with $^{234}U/^{238}U$~1.15 (e.g. Ku et al., 1977). Therefore, in waters, and in authigenic minerals younger than ~1 Ma precipitated from seawater or other water bodies, we expect to see $^{234}U/^{238}U > 1$ (e.g. Porcelli and Swarzenski, 2003). In small water bodies such as rivers and lakes, $^{234}U/^{238}U$ ratios are affected by lithology, the period of water-rock interaction, physical or chemical weathering, and occurrence of secondary minerals.

The $^{234}U/^{238}U$ in the modern Dead Sea of ~1.45 reflects its sources (Haase-Schramm et al., 2004). Authigenic minerals record the $^{234}U/^{238}U$ of the lake through time. Gypsum and aragonite incorporate uranium from the Dead Sea water in the mineral lattice, while in halite the uranium comes from Dead Sea water and gypsum inclusions (Kiro et al., 2016). Aragonites from the Holocene show initial $^{234}U/^{238}U$~1.45 (Torfstein et al., 2015). During the last glacial period, when lake levels were high (Bartov et al., 2003, 2002), $^{234}U/^{238}U$ ratios in precipitated aragonites show values

similar to the Holocene (1.51 ± 0.01). In water sources in the northern part of the Dead Sea watershed (e.g. the Jordan River) and western catchment springs, $^{234}U/^{238}U$ varies between ~1.4–1.7 (Haase-Schramm et al., 2004). Because fresh water entering the lake has higher discharge rates and higher U concentrations compared with brines, these variations in the $^{234}U/^{238}U$ ratio mainly reflect changes in the freshwater input. The differences in $^{234}U/^{238}U$ between aragonite deposited during the last glacial period and the Holocene are small, because both reflect the Jordan River as the main source of water to the lake.

1.4. Paleoclimate interpretations using $^{234}U/^{238}U$ isotope ratios

In this section, we explain why the changes in the $^{234}U/^{238}U$ ratios in the Dead Sea core reflect changes in sources and/or frequencies of flash floods by discussing processes that impact these ratios in natural waters. While $^{234}U/^{238}U$ ratios have been used for paleoclimate interpretations associated with changes in precipitation (e.g. Frumkin and Stein, 2004; Robinson et al., 2004), its application is not straightforward and it must be used with caution. Understanding regional effects on $^{234}U/^{238}U$ ratios in water sources is important for interpreting its paleoclimate implications (Robinson et al., 2004). Lithology, physical and chemical weathering, soil cover, and the mode and amount of rainfall are important factors impacting $^{234}U/^{238}U$ ratios in water (e.g. Frumkin and Stein, 2004; Hellstrom and McCulloch, 2000; Kaufman et al., 1998; Porcelli and Swarzenski, 2003; Robinson et al., 2004).

Due to the variability of geographical settings, surface lithology, and climate, the factors that affect U-isotopes in water vary in different regions. For example, high rates of physical weathering in major mountain ranges expose fresh rock surfaces to chemical weathering, whereby ^{234}U in lattice sites damaged by alpha-recoil are preferentially available for dissolution into groundwater and runoff compared to ^{238}U, as shown by the positive relationship between uplift rates and $^{234}U/^{238}U$ in New Zealand rivers (Robinson et al., 2004). The mode of rainfall also impacts $^{234}U/^{238}U$ values. Flash floods around the Dead Sea often show low $^{234}U/^{238}U$-values of ~1.15–1.30 (Table S2), reflecting short water-rock interactions (compared with the high activity ratio of 1.5–1.7 of groundwater discharging from carbonates), which is also reflected in low values in some speleothems (Grant et al., 2012).

The amount of precipitation has also been suggested to affect the $^{234}U/^{238}U$ ratio. Decreasing rainfall rates allow ^{234}U to accumulate in rocks and soils, leading to higher $^{234}U/^{238}U$ in groundwaters and runoff, while increased rainfall rates have the opposite effect (Robinson et al., 2004) by more efficiently washing away the more labile ^{234}U. Following this rationale, increased rainfall rates have been invoked to explain decreases of $^{234}U/^{238}U$ during the last deglaciation (Hellstrom and McCulloch, 2000; Robinson et al., 2004). On the other hand, in speleothems in Israel, higher $^{234}U/^{238}U$ has been interpreted to reflect increased rainfall (Frumkin and Stein, 2004). Their explanation is that in the Levant, more rainfall results in increased dust accumulation and soil generation, which increases sources of labile ^{234}U for dissolution. This means that the direction of the changes in $^{234}U/^{238}U$ ratios with increasing rainfall depends on regional conditions.

While changing the amounts of rainfall impact $^{234}U/^{238}U$ ratios in both New Zealand and Israel, the degree of change is small compared to the range in the DSDDP cores. In both cases, the $^{234}U/^{238}U$ variability in response to changes in rainfall amount is ~0.07–0.13 activity units. The change in Soreq Cave speleothems range between ~1.02–1.08 (Grant et al., 2012; Kaufman et al., 1998) while in New Zealand the range is between ~1.43 and ~1.37. In the Dead Sea mineral precipitates during MIS 5e the values vary between ~1.5 and ~1.0, a change of 0.5 activity units (Figs. 2 and 3, Table S2). This large range in the Dead Sea is similar to the variability in its water sources, driven by the different lithologies, thus providing evidence that the changes observed in this study reflect provenance rather than weathering intensity (details on the provenance are in Results Section 4.1). Although the effects of rainfall amount on $^{234}U/^{238}U$ ratios in water sources are small compared to provenance differences, they were taken into account when calculating the U budget (Section 4.1.1).

2. Chronology of the DSDDP core

The initial age-depth model of the DSDDP core (Torfstein et al., 2015) used a combination of indicators, including 1. ^{14}C dating of organic remains, 2. U-series dating of DSDDP aragonite, 3. comparisons between $\delta^{18}O$ in DSDDP aragonite and the LR04 benthic stack chronology (Lisiecki and Raymo, 2005) and Soreq Cave speleothems dated by U–Th disequilibrium (Bar-Matthews et al., 2003; Grant et al., 2012), and 4. correlation between distinctive sedimentary layers in the core and subaerial sediments near Dead Sea that were previously dated to high precision by U–Th disequilibrium (Haase-Schramm et al., 2004; Torfstein et al., 2009). It used nine anchor age points for the entire 456 m of core and assumed a linear interpolation in between. An updated chronology (Goldstein et al., 2020, this volume) that tunes the age-depth model more precisely and uses many more tie points, is based on the large amount of information gathered in the intervening time on the DSDDP core material, including many more ^{14}C ages, more $\delta^{18}O$ analyses on aragonites, identification of additional correlative sedimentary layers between the DSDDP core and marginal deposits, and tuning of DSDDP aragonite $\delta^{18}O$ variations with and U–Th dated Soreq Cave speleothems and mid-latitude summer insolation variations.

During the MIS 6/5 transition through MIS 5e, the time period relevant to this study, in the initial age-depth model (Torfstein et al., 2015) the MIS 5e ages were defined by three anchor points at 135, 123, and 117 ka linked to the MIS 6/5 deglaciation, the MIS 5e peak, and the end of the major salt deposition, respectively. These were determined by comparison of $\delta^{18}O$ changes in the core with the corresponding changes in the LR04 benthic stack (Lisiecki and Raymo, 2005) and U–Th dated Soreq Cave speleothems (Bar-Matthews et al., 2003; Grant et al., 2012). That model was supported by two U–Th analyses of an aragonite layer within the MIS 5e that yielded an age of 117.4 ± 2.6 ka, consistent with its depth but with a high uncertainty; the age at the same depth in the updated chronology is 117.2 ka. An additional (failed) attempt within MIS 5e showed highly variable U–Th ages and was discounted.

The updated model (Goldstein et al., 2020, this volume) is based on comparison of the $\delta^{18}O$ in the DSDDP core (including additional aragonite $\delta^{18}O$ analyses) and the Soreq Cave speleothems using Bar Matthews et al. (2003). This approach is justified because both the Soreq speleothems and the DSDDP aragonite $\delta^{18}O$ records follow the changes in the Mediterranean $\delta^{18}O$ (Kolodny et al., 2005). The ages are constrained by 4 tie-points on the prominent MIS 5e $\delta^{18}O$ peak in both records (Fig. S1); at each end of the MIS 5e peak (136 and 116 ka) and on the flanks (129 and 119 ka) (Table 1), with estimated uncertainties less than 1000 years (Goldstein et al., 2020, this volume). The close relationship between the changes in $\delta^{18}O$ in DSDDP core aragonites and Soreq speleothems during MIS 5e adds confidence to the age-depth model. While over the entire core there are some substantial differences between the two age models, as high as ~13 kyr, during MIS 5e the two age-depth models are in substantial agreement, with a maximum difference of 2.6 kyr (Fig. S2).

We further performed a Monte Carlo simulation (Table 1), which applied a range of ages to depths in the Dead Sea DSDDP core, in a

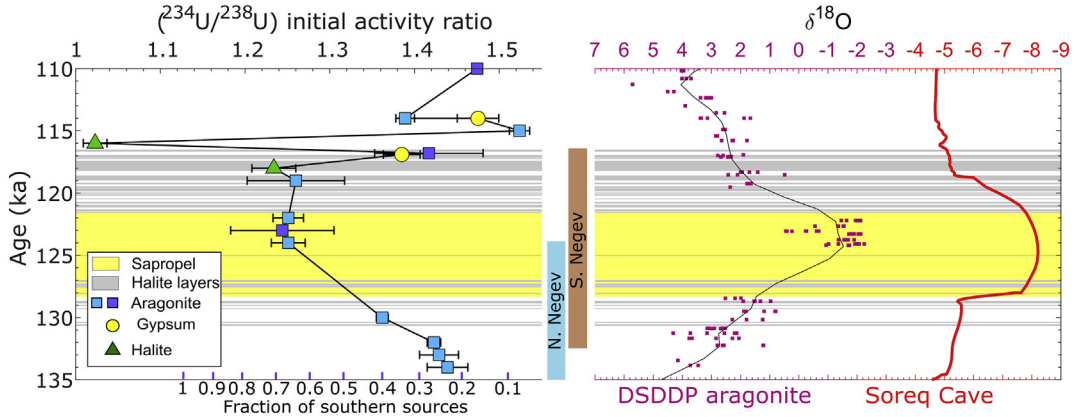

Fig. 3. Blow up of MIS 5e $^{234}U/^{238}U$ in the context of the salt layers (gray), sapropel S5 (yellow), the calculated fraction of southern sources, the occurrence of south (brown) and north (blue) Negev speleothems, and the Soreq Cave $\delta^{18}O$. Plotted points are the average and error bars are 2σ-mean of the samples from the same depth in Fig. 2A. (For interpretation of the references to colour in this figure legend, the reader is referred to the Web version of this article.)

Table 1
DSDDP age model tie points, Monte Carlo ages, and major lithology transitions during MIS 5e. Standard deviations are estimated according to all acceptable MC age models that meet the threshold.

Depth (m)	Manually selected tie point (ka)	MC age for tie point (ka)	SD (1σ)	Threshold for acceptable age model in the Monte-Carlo simulation
357.2	150	150.5	2.1	$\chi^2<1$, $r^2>0.65$, PCC>0.65, $p < 0.1$
328.87	136	135.7	0.2	$\chi^2<1$, $r^2>0.65$, PCC>0.65, $p < 0.1$
316.24	129	129.2	0.05	$\chi^2<1$, $r^2>0.65$, PCC>0.65, $p < 0.1$
258.18	119	119.2	0.1	$\chi^2<1$, $r^2>0.65$, PCC>0.65, $p < 0.1$
230.31	116	114.9	0.9	$\chi^2<1$, $r^2>0.65$, PCC>0.65, $p < 0.1$
222.96	112	111. 3	0.4	$\chi^2<1$, $r^2>0.65$, PCC>0.65, $p < 0.1$
Lithology Transitions				
Depth (m)	Age model (ka)	MC age (ka)	SD (1σ)	Remarks
320.05	130.6	130.7	0.21	Beginning of first MIS 6/5 halite sequence
304.53	127.0	127.2	0.98	Beginning of S5 wet interval
279.11	121.5	121.8	0.1	End of wet S5 interval
233.25	116.5	115.8	0.8	End of thick halite sequence

uniform distribution according to the possible fits of the DSDDP core aragonite $\delta^{18}O$ values to the Soreq speleothem calcite $\delta^{18}O$. A linear regression model is applied to all possible age models in the Monte Carlo simulation. The goodness of fit is tested by a χ^2 goodness of fit test, the Pearson Correlation Coefficient (PCC), coefficient of determination (r^2) and the probability value of the significance of the linear correlation. These methods are commonly used for age modeling and wiggle-matching (e.g. Ramsey et al., 2001). The Monte Carlo results agree with the manually selected tie points within 200–1100 years, well within the uncertainties of both approaches (Table 1 and Goldstein et al., 2020, this volume). According to the new age model (Goldstein et al., 2020), the beginning of the relatively wet interval is 127 ka, the transition between MIS 5e wet interval and the arid phase (reflected by the thick late MIS 5e sequence of halite) is at 121.5 and the end of the arid period is at 116.5.

3. Methods

Sampling: Samples were collected from all of the visible layers of aragonite, gypsum (100 mg) and halite (10 g). Halite samples were taken at the end of MIS 5e (233-235 m depth in the DSDDP core), and from the middle of the thick halite sequence at the end of MIS 5e. The depths of the samples are listed in Table S1. The depth of a halite sample denotes the bottom of the sample (~10 cm from a ~1 × 2 cm slab). Each aragonite and gypsum sample is from a single lamina. Duplicated samples are from adjacent laminae.

Analyses: Uranium isotopes, and U and Nb concentrations, were measured on primary aragonite, gypsum and halite samples from the DSDDP core. Niobium is an insoluble element and was used as a monitor of the amount of detritus in each sample, in order to correct for detrital U. The impacts of detrital U on our data are small, as explained in Supplementary Materials.

Sample processing: Samples were processed for chemical analysis in the ultra-clean chemistry lab at Lamont-Doherty Earth Observatory of Columbia University (LDEO). Aragonite and gypsum (~100 mg) were rinsed 3 times with Milli-Q® water in order to remove soluble salts, and then digested completely using HNO_3 and HF. Halite (~10 g) was dissolved in water, and HNO_3 and HF were added to dissolve any detritus. Detritus (~100 mg) samples were leached for carbonates using 1N HCl, followed by 3 rinses of Milli-Q® water. Water samples were collected in 0.5–2 L bottles and were separated from particulates by 0.45μ filters and centrifuging. The water samples were acidified with HCl to pH~2. The U was co-precipitated with iron from the water and halite samples by using 4 mg of clean $FeCl_2$ per liter of solution, by adding ammonium hydroxide into the solution and adjusting the pH to 8.5–9. The precipitates were centrifuged and rinsed three times with Milli-Q® water. All water samples that were collected reflect natural sources and are not affected by anthropogenic contamination, which is also indicated by the major element chemistry.

For separation of U, samples were loaded in 2 ml 7N HNO_3 onto columns filled with 2 ml of AG1X8 200–400 mesh anion exchange resin. Uranium was eluted using 1N HBr. A spike containing ^{233}U

and ^{236}U was added before digesting and dissolving the samples in order to determine U concentrations.

Analytical measurements: U concentrations and $^{234}U/^{238}U$ ratios were measured using a ThermoScientific Neptune Plus® multicollector ICP-MS at LDEO in solutions with 100–300 ppb U. Samples were introduced through an ESI APEX® micro-concentric desolvating nebulizer sample introduction system. ^{238}U, ^{236}U, ^{235}U and ^{233}U were measured on Faraday cups with 10^{12} Ω resistors for ^{235}U, ^{236}U and ^{233}U and a 10^{11} Ω resistor for ^{238}U. ^{234}U was measured on a multiplier with an RPQ filter. Mass fractionation was corrected to a $^{238}U/^{235}U$ atomic ratio of 137.88 using the exponential mass fractionation law. The multiplier-Faraday gain was calibrated using Certified Reference Material (CRM) 145 (New Brunswick Laboratory, U.S Department of Energy) measured between samples. The $^{234}U/^{238}U$ external 2σ standard deviation is typically 0.2–0.3% (based on 20 to 50 measurements of the standard per session), but in all cases lower than 0.6%. Niobium concentrations were measured by a VG PQ ExCell® quadrupole ICP-MS at LDEO. Errors of trace element concentrations are estimated to be ~2%, based on multiple runs of a calibration curve from measurement of in-house multi-element solutions and rock standards.

Climate model simulations: The climate model results presented in this study are from existing simulations that were performed at the National Center of Atmospheric Research (NCAR) and obtained courtesy of Dr. Bette Otto-Bliesner as part of the Paleoclimate Model Intercomparison Project phase 3 (PMIP3). In these last interglacial simulations, the coupled Community Climate System Model version 3 (CCSM3) was forced with insolation corresponding to orbital conditions at 130, 125 and 120 ka. The CCSM3 is an intermediate resolution model with the atmosphere represented by a longitude and latitude grid spacing of ~1.4° and 26 levels in the vertical. The ocean model component had a 1° horizontal resolution and 40 levels in the vertical. The model includes a land surface model with specified, spatially dependent land cover types. The model uses present-day geography with present-day Greenland and Antarctic ice sheets and vegetation. To compare to present-day climate, we used an extended pre-industrial (PI) simulation with the same model time averaged in the same manner. Atmospheric CO_2 where set to 273, 272 and 289 ppmv for the 125 ka, 120 ka and PI runs, respectively, according to the ice core records. Each pre-industrial simulation was run for over 300 years and the mean climate in each time section was determined by averaging over the last 30 years of these runs. The details of the simulation parameters and discussion of the results as per their expression in the distribution of surface air temperature around the globe and by season, as well as a comparison with paleoclimate observations, are summarized in Otto-Bliesner et al., (2013).

4. Results and discussion

Our results include new $^{234}U/^{238}U$ ratios in the DSDDP core mineral precipitates and detritus, and Dead Sea water sources (Tables S1, S2 and S3, Figs. 2 and 3), a U isotope budget and calculated southern/eastern runoff to the Dead Sea (Sections 4.1.1 and 4.1.2), and a presentation of climate model results (e.g. precipitation and temperature) in the Levant during 125 and 120 ka (Fig. 4 and Supplementary Material).

4.1. Dead Sea water sources shifts indicated by $^{234}U/^{238}U$ ratios

In the western catchment, the most important fresh to brackish spring sources, discharging primarily from carbonate rocks, have high $^{234}U/^{238}U$-values of ~1.45–1.75, similar to the Jordan River flowing from the north with values of ~1.45, while the main water sources in the eastern and southern catchment, discharging mainly from Paleozoic and Mesozoic silicate sedimentary rocks, and flash floods that are typical for the desert south, have much lower $^{234}U/^{238}U$ values of ~1.08–1.19 and 1.15–1.3, respectively (Fig. 1), (excluding two samples from two streams with high $^{234}U/^{238}U$ but insignificant water flux).

In general, the $^{234}U/^{238}U$ ratios in the Dead Sea water sources have been consistent in space and time, at least on the time-scale of several years, and have not varied (by more than 0.2 activity units) as a function of runoff (Table S2). Samples from different streams and springs with a large discharge range show similar $^{234}U/^{238}U$ values, which mainly depends on two factors: (1) the lithology of the rock that the water is discharging from (silicate rocks vs. limestone), and (2) the time interval of water-rock interaction. All water samples from the eastern catchment, that discharge out of silicate rocks, contain relatively low $^{234}U/^{238}U$, while water discharging from the north (feeding the Jordan River) and west from carbonate contain relatively high $^{234}U/^{238}U$. In addition, flash floods, usually associated with precipitation in the south and east, also contain low $^{234}U/^{238}U$, both in the eastern and western catchments of the Dead Sea. There is a consistency between the $^{234}U/^{238}U$ values in the eastern catchment sources (all discharging from silicate rocks), despite the large range of fresh water discharge in between the different sources (a few to ~100 million m^3/y). The changes between the water interacting with carbonates (in the western catchment and the Jordan River sources) and water interacting with more silicate compositions (in the eastern catchment) reflect mainly the differences in lithology. Groundwater discharging out of silicates and water experiencing relatively short water-rock interaction (in speleothems and flash floods) contain lower $^{234}U/^{238}U$ ratios (~1.0–1.3) and groundwater discharging out of carbonates contain higher ratios (~1.45–1.7).

Our new data (79 new $^{234}U/^{238}U$ analyses on the DSDDP core sediments between 160 and 90 ka, plus 9 new analysis of Dead Sea water sources) show that during different intervals of MIS 5e, $^{234}U/^{238}U$ ratios were dramatically different (Figs. 2 and 3, Table S1). From typical values of ~1.5, they declined to ~1.3 during the MIS 5e insolation peak/Sapropel 5/African wet period between 127–122 ka, and were as low as ~1.0–1.1 at the end of the dry period that followed at ~122116 ka, signaling relative decreases in the input from Jordan River-western catchment sources. The overall trend during MIS 5e towards these extreme low $^{234}U/^{238}U$-values is interrupted by an abrupt increase to typical Dead Sea values of ~1.45–1.55 just before the shift to ~1.0 (Fig. 3), which reflects a short episode with input from the Jordan River.

The observed $^{234}U/^{238}U$ shifts indicate unique climate and environment conditions during intervals within MIS 5e. The $^{234}U/^{238}U$ ratio of Dead Sea water and its mineral precipitates today of ~1.45 (Table S2) is nearly the same as the value of ~1.5 observed through the last ice age (MIS 2–4) (Haase-Schramm et al., 2004), when the climate was wetter and the lake level was up to 240 m higher than the Holocene norm of ~400 mbsl. This near constant value has held over most of the 200,000 year DSDDP record. It mainly reflects the $^{234}U/^{238}U$ ratio of the Jordan River whose source is the mountains to the north and its constancy as the main water source for the Dead Sea, despite the large lake level changes that have occurred as well as large changes in the amount of rainfall.

This general glacial-interglacial variability between ~1.45–1.55 (~0.1 activity units) is much smaller than the large shift of the $^{234}U/^{238}U$ ratios to ~1.3 during the MIS 5e insolation peak, and to 1.0 during the late MIS 5e dry period (Figs. 2 and 3). As already noted, these shifts (0.2–0.5 activity units) are also much greater than the effects from changing rainfall rates observed in speleothems (0.05–0.1 activity units). Rather, they must be reflecting more fundamental shifts in the sources of uranium. Our water sources survey (Table S2, Fig. S5), along with published $^{234}U/^{238}U$ and other

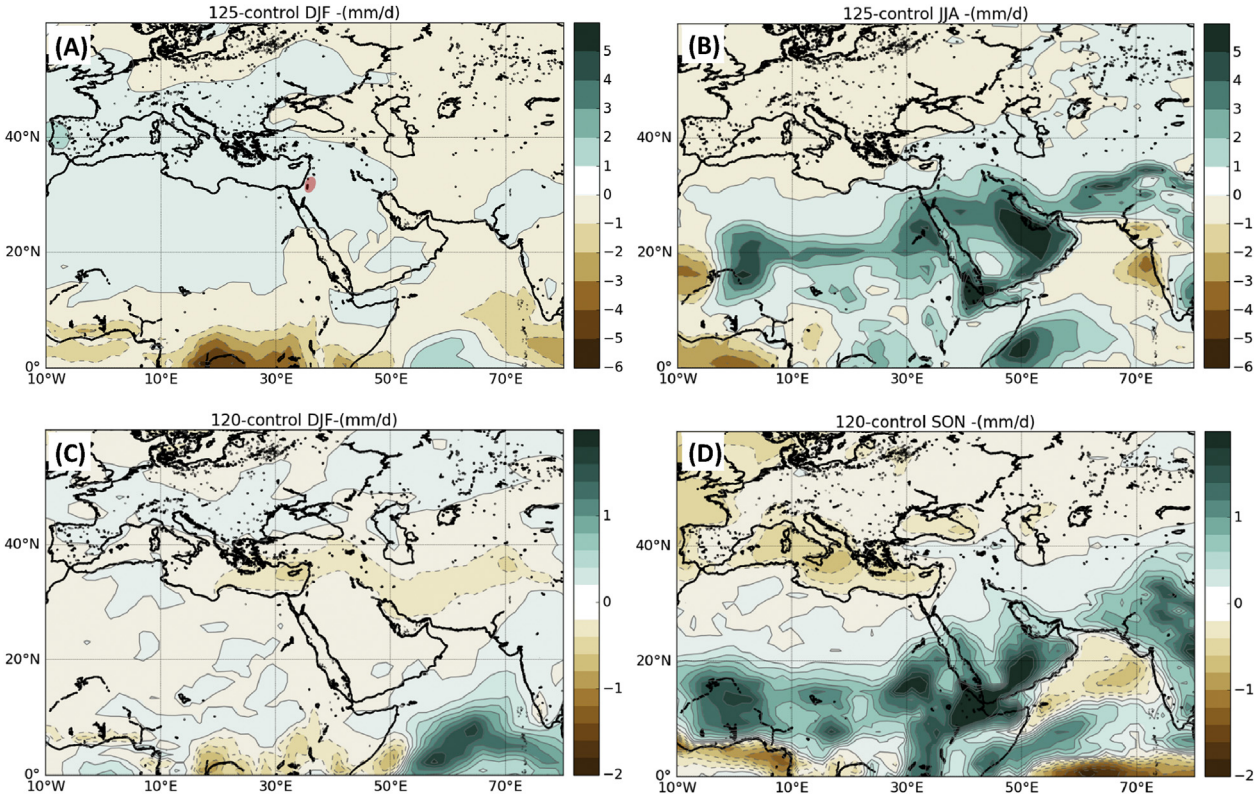

Fig. 4. Precipitation anomaly relative to present-day from CCSM3 models (Otto-Bliesner et al., 2013) for (A) winter (DJF) precipitation at 125 ka, B) summer (JJA) precipitation at 125 ka, C) winter (DJF) at 120 ka, and D) autumn (SON) at 120 ka. The annual precipitation is higher than today at 125 ka. At 120 ka the winter is drier than today and the autumn is wetter. The Dead Sea basin is marked in red. Note that the precipitation scale is different in each one of the maps. Annual precipitation during 120 and 125 ka, and the difference between 125 and 120 ka are in the supplementary material in Figure S6. (For interpretation of the references to colour in this figure legend, the reader is referred to the Web version of this article.)

radionuclides data (Haase-Schramm et al., 2004; Kiro et al., 2015; Kronfeld et al., 1991), show that the biggest variations in the $^{234}U/^{238}U$ ratios of Dead Sea water sources (Fig. 1) are related to the lithology of the rocks of the tributaries, and the effects of flash flooding. In this context, the large Dead Sea $^{234}U/^{238}U$ shifts during parts of MIS 5e reflect the low values associated with flash flooding events, and the low values of the water sources in the southern-eastern catchments, as opposed to the high values of the Jordan River and western catchments. Thus, the lower $^{234}U/^{238}U$ ratios must reflect a relative decrease in the Jordan River sources versus others, and the late MIS 5e values of ~1 must reflect a near shut-down of the Jordan River. Nevertheless, the possible variations in the water sources due to changing rainfall are included in the uncertainty in the U budget in the next section.

4.1.1. U isotope and water budget in the Dead Sea

For each U isotope under steady-state conditions, the following equation applies:

$$\sum_i F_i \cdot U_i = F_{out} \cdot U_{DS} \tag{1}$$

where F [L^3/T] and U [M/L^3] are the water discharge and the concentration of the uranium isotope, respectively, and subscripts i, *DS* and *out* refer to the specific water source, the Dead Sea and removal flux, respectively. Thus,

$$\frac{\sum_i F_i \cdot {}^{234}U_i}{\sum_i F_i \cdot {}^{238}U_i} = \left(\frac{^{234}U}{^{238}U}\right)_{DS} \tag{2}$$

As a simplification, we consider two main sources, which allows us to calculate the fraction of the source contributing low $^{234}U/^{238}U$ ratios to the Dead Sea (i.e. the south-east water sources and/or flash floods). Assuming that U concentration is ^{238}U concentration:

$$\frac{F_S}{F_T} = \frac{U_N\left[\left(\frac{^{234}U}{^{238}U}\right)_{DS} - \left(\frac{^{234}U}{^{238}U}\right)_{N}\right]}{\left(\frac{^{234}U}{^{238}U}\right)_{S}\cdot U_S - \left(\frac{^{234}U}{^{238}U}\right)_{N}\cdot U_N - \left(\frac{^{234}U}{^{238}U}\right)_{DS}\cdot(U_S - U_N)} \tag{3}$$

where F_S [L^3/T] and F_T [L^3/T] are the southern/eastern/flash flood water discharge and total water discharge, respectively. U_N [M/L^3] and U_S [M/L^3] are the uranium concentrations in the north/western catchment sources and the southern/eastern/flash floods sources, respectively. The *N, S, DS* subscripts in the isotopic ratios refer to north, south and Dead Sea.

This equation resolves the fraction of the southern source from the total source, i.e. the relative flux of north and west vs. south and east. There are no assumptions on the total runoff or changes in

Table 2
U concentrations and $^{234}U/^{238}U$ used in the budget calculation.

Parameter	avg.	1σ
U_S (ppb)	0.92	0.1
U_N (ppb)	0.7	0.1
$(^{234}U/^{238}U)_S$*	1.13	0.02
$(^{234}U/^{238}U)_N$*	1.57	0.03

Table 3
Parameters used for budget calculation and U budget results. MIS 5e drought includes two scenarios, with $^{234}U/^{238}U = 1.25$ and $^{234}U/^{238}U = 1.05$

	$(^{234}U/^{238}U)_{DS}$		% F_S		F_S (million m^3/y)		F_T (million m^3/y)	
	avg.	1σ	av.	1σ	av.	1σ	av.	1σ
Present-day	1.46	0.01	20	6	333	122	1650[a]	350
Last glacial	1.5	0.03	12.5	8	406	254	3250[c]	250
MIS 5e drought (120 ka)	1.25	0.03	50	17	361	69	720[b]	60
	1.05	0.015	95	9	687	85	720[b]	60
MIS 5e peak (125 ka)	1.3	0.033	55	10	1099	287	2000[b]	350

[a] (Lensky et al., 2005; Salameh and El-Naser, 1999).
[b] (Kiro et al., 2017).
[c] Estimated roughly from the Dead Sea hypsometric curve (Hall, 1997) and last glacial lake levels (Bartov et al., 2002). F_s is the flux from flash floods and the southern and eastern catchments, and F_T is the total water flux. DS is Dead Sea.

precipitation.

Table 2 summarizes the concentrations and $^{234}U/^{238}U$ activity ratio and their uncertainties that were used to calculate the fraction of the two sources by equation (3). These include the ranges observed in all the eastern catchment sources and floods (with the typical lower activity ratios) and the northern and western catchment (with the typical higher activity ratios) that are shown in Table S2.

S represents the southern and eastern catchments plus flash floods, N represents the northern and western catchments. *Values for the late MIS 5e drought are 1.03 ± 0.03 and 1.54 ± 0.03, for consistency with the low ratios in the lake at that time and the estimated effect of the dry period on the composition of the sources (Frumkin and Stein, 2004).

The results of the budget and the Monte-Carlo uncertainty analysis are summarized in Table 3. For the Monte-Carlo analysis, the U concentrations and isotope ratios, and the total runoff amounts are estimated to have a normal distribution with a standard deviation (1σ) covering the range of values in Tables S1 and S2. The calculated percent of the southern and eastern sources (% F_S in Table 3) is a direct result of the Monte-Carlo analyses of equation (3).

The water budget from the Jordan River and the southern/eastern catchments can be estimated *combining* the relative fluxes with the estimated total fluxes (Table 3). In order to estimate the actual runoff of the northern/western and eastern/southern water sources we estimated discharge of the different water sources based on previous studies (Lensky et al., 2005; Salameh and El-Naser, 1999) and evaporation rates (Lensky et al., 2005; Stanhill, 1994).

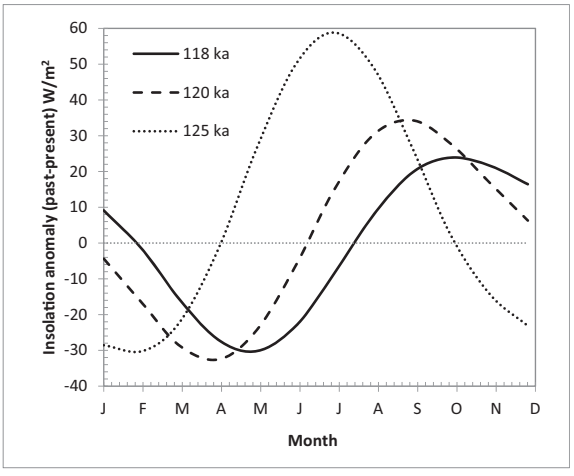

Fig. 5. Monthly insolation anomaly (past minus present) at 30°N (Paillard et al., 1996) during the last interglacial. The maximum positive anomaly shifts from summer at 125 ka towards the autumn at 120 ka.

The present-day (pre-1964) total runoff is estimated to 1600–2000 million m^3/y from estimates of all of the water sources to the Dead Sea. The evaporation rate of the Dead Sea during that time is estimated to 1.3–1.9 m/y (Stanhill, 1994). Given a surface area of 950 km^2, the steady-state runoff is 1235–1805 million m^3/y. This small discrepancy may be due to evaporation of water from the watershed before entering the Dead Sea.

The total runoff during the MIS 5e peak (~127122 ka) is estimated based on the Mg concentration in pore waters during that time (Kiro et al., 2017; Levy et al., 2016). The lake level at the MIS 6/MIS 5 transition was −320 m (Kiro et al., 2017) with Mg of 0.9 mol/kg H_2O, which reached 1.3 mol/kg H_2O at the MIS 5e peak. Since Mg can be considered as conservative, this change in concentration directly reflects the change in lake volume (from ~240 to ~170,10^9 m^3). Using the Dead Sea hypsometric curve (Hall, 1997), this corresponds to a lake level of ~ -370 m, which corresponds to a runoff of ~1600–2400 million m^3/y.

The runoff during late MIS 5e (~122116 ka) is taken from Kiro et al. (2017). The annual variability in rainfall in this region is high with a 35% standard deviation, and very dry years with annual precipitation below 40% of the average. The estimated decrease of 50–70% in the average precipitation during that time interval suggests that dry years were more frequent.

The uranium isotope budget for the present-day lake agrees with the known sources estimated independently, which indicate that all the significant sources of uranium are included in our budget. The present-day southern source (F_S), fed by both Mediterranean and southern climate systems, includes both eastern catchment perennial flow (~250 million m3/y), groundwater from the eastern catchment (~50 million m3/y) and flash floods (~50 million m3/y) (Lensky et al., 2005; Salameh and El-Naser, 1999).

4.1.2. The Dead Sea catchment water budget during MIS 5e

The U-isotope budget shows that at the peak of MIS 5e, ~55% of the Dead Sea water sources came from southern/eastern catchments and/or flash floods, with a runoff amount that is ~3 times the present-day southern/flood runoff. During late MIS 5e, 50% and then >90% of the water sources were southern/eastern catchments and/or flash floods, thus with almost no contribution from the Jordan River. The total contribution from southern/eastern sources and/or floods was higher than the present-day, reaching twice the current runoff. These increases in precipitation probably resulted in higher runoff of the perennial flows in the eastern catchment (Wadis Mujib, Hasa, and Zarka Main, Fig. 1, S3) and an increase in the frequency of flash floods. Since the precipitation is already low in the eastern catchment (<200 mm/y, Fig. 1), the increase in precipitation that doubles or triples the runoff, is not a drastic change in the total runoff, and is not expected to change the $^{234}U/^{238}U$ ratio

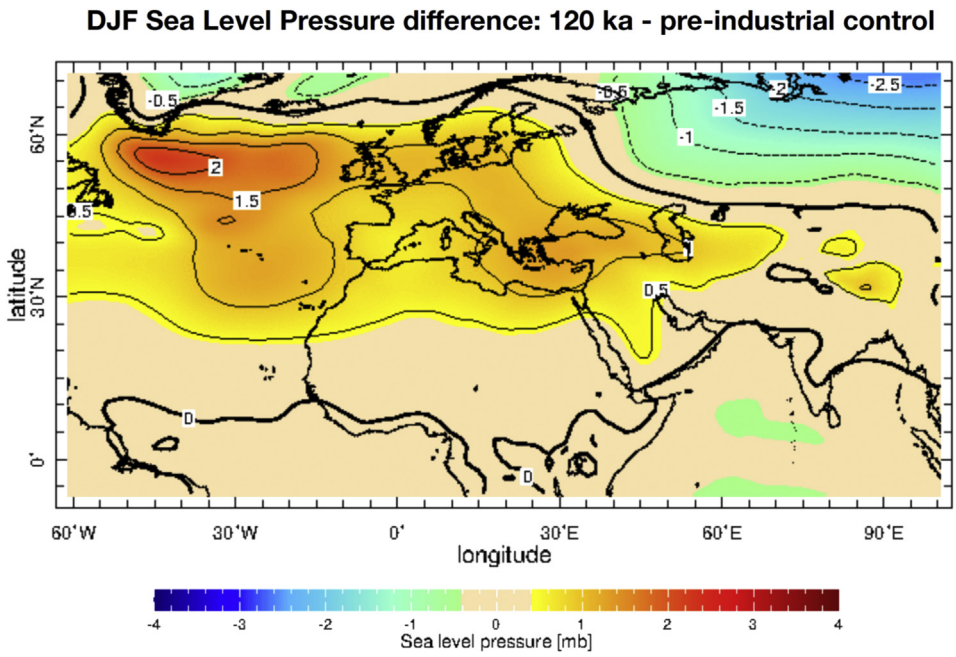

Fig. 6. Sea level pressure differences between 120 ka and today (pre-industrial) during winter in the CCSM3 climate model results (Otto-Bliesner et al., 2013), showing high pressure above the North Atlantic, Europe and the Mediterranean.

of the sources more than 0.05 activity units.

The $^{234}U/^{238}U$ shifts to low values evidence a decrease in the Jordan River flux, thus signaling weakening of the Mediterranean winter storm systems that bring the bulk of present-day moisture, and a shift of the primary moisture sources to the south. Moreover, the $^{234}U/^{238}U$ ratios close to ~1.0 during late MIS 5e (after 120 ka) evidence a significant weakening of the Mediterranean systems over the Levant. Such a change in the moisture sources has been suggested in some previous studies, but solid evidence has been lacking until now, and thus the idea that there was a shift toward moisture sources from the south to the Dead Sea basin has been highly debated (Battisti et al., 2014; Douady et al., 2003; Drake et al., 2011; Kutzbach et al., 2014; Lahr and Foley, 1994; Orland et al., 2019). In addition to the $^{234}U/^{238}U$ data, CCSM3 climate model simulations of MIS 5e support the shift to larger contributions from south of the Dead Sea basin (Fig. 4 and discussion below).

4.2. Levant records of last interglacial hydroclimate shifts

The high-resolution record of the DSDDP cores provides a detailed description of the hydroclimatic characteristics, which are partly reflected in the regional speleothem records. Speleothems in Soreq Cave near Jerusalem (Bar-Matthews et al., 2003), in the Mediterranean climate zone, and in the Negev desert (Vaks et al., 2010, 2006) (locations are in Fig. 1) indicate wetter conditions than today during the last interglacial insolation peak, ~127–122 ka, which is also seen in the DSDDP core. Moreover, the evidence of increased precipitation in the Soreq speleothems, indicated by low $\delta^{18}O$-values, ends at the beginning of the DSDDP extreme drought interval, at ~120 ka, together with the termination of speleothem growth in the Northern Negev (Fig. 2). This indicates that the Southern Negev remained relatively (compared to its typical conditions) wetter, while the Northern Negev returned more similar to its typical state.

As for the source of moisture, some studies have concluded that the sources are tropical (e.g. Orland et al., 2019), while others have favored the Mediterranean (e.g. Bar-Matthews, 2014). It turns out that taking into consideration the DSDDP cores along with the Negev speleothem data resolves this apparent discrepancy in favor of both of them. The high-resolution $^{234}U/^{238}U$ data in the DSDDP record (Fig. 2), which reflect the changes in the water sources to the Dead Sea, indicate that during the peak insolation interval of MIS 5e, between 127 and 122 ka, rainfall was fed by both Mediterranean and tropical moisture sources. The low $\delta^{18}O$-values in the Negev speleothems (Vaks et al., 2006), along with an observed decrease in the thickness of speleothem layers from north to south, led Vaks et al. (2010) to conclude that the Mediterranean was the source of the moisture to the Levant during most of that time interval. Nevertheless, they could not rule out tropical moisture sources (Vaks et al., 2006). The intermediate $^{234}U/^{238}U$-values during this interval in the DSDDP record of ~1.2–1.3 (Figs. 2 and 3), significantly below the norm of ~1.45–1.55 and higher than the extreme values of 1.0 at the end of MIS 5e, coincided with speleothem growth in both the north and south Negev, indicating that the Mediterranean was a significant source of moisture, feeding runoff via the Jordan River, but that a tropical source was also present. Subsequently, during the extreme drought interval after 120 ka, when the Dead Sea $^{234}U/^{238}U$-value decreased to ~1.0, the northern Negev speleothems ceased to grow while the speleothems in the southern Negev continued growing, documenting continued moisture in the south and drier conditions in the north. Moreover, the conditions in the north were dry enough that the contribution of uranium from the Jordan River to the Dead Sea became insignificant.

The extreme low $\delta^{18}O$-values in the regional speleothem records during the MIS 5e insolation peak interval (127–122 ka) is also seen in the Dead Sea mineral precipitates. The Soreq Cave $\delta^{18}O$-values show unusually large deviations from the Eastern Mediterranean (Fig. 2). Present-day rainwater $\delta^{18}O$-values negatively correlate with the amount of annual rainfall at Soreq, and the low $\delta^{18}O$-values have been interpreted to indicate high amounts of Mediterranean-sourced rainfall (Bar-Matthews et al., 2003).

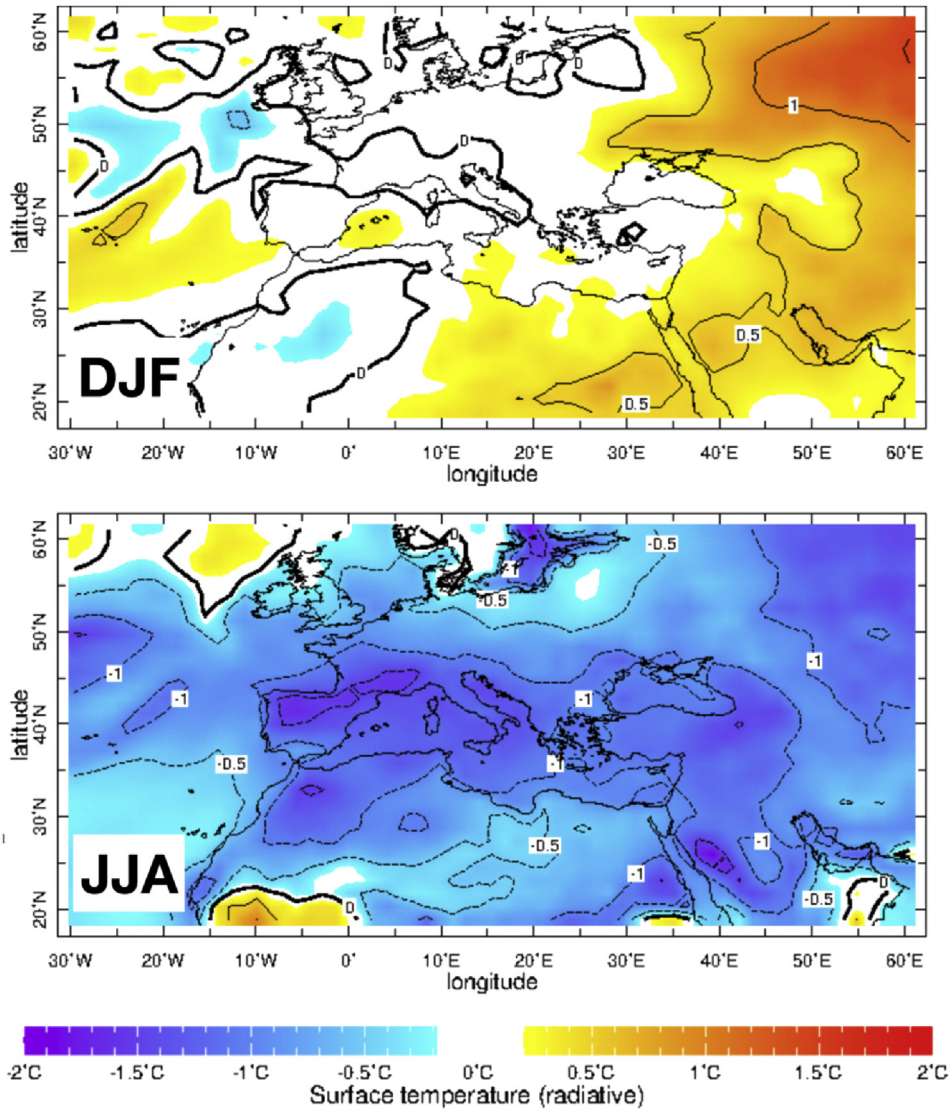

Fig. 7. Winter (top) and summer (bottom) temperature differences between 120 ka and today (pre-industrial) in the CCSM3 climate model results (Otto-Bliesner et al., 2013), showing that winter was warmer, summer was colder.

However, low δ^{18}O-values may alternatively indicate more intense rainfall events, and low coeval δ^{13}C-values in Soreq speleothems have been interpreted to reflect intense water flow (Bar-Matthews et al., 2003). As an additional alternative, low δ^{18}O-values could also reflect moisture from more distal tropical sources as a result of Rayleigh distillation of condensing humidity over long transport distances (Gat and Carmi, 1987). Moreover, even when the source of rainfall is tropical or subtropical, a synoptic system carrying the moisture will pick up Mediterranean moisture if it reaches there, as seen today (de Vries et al., 2013), which would contribute to the δ^{18}O-values of the speleothems. Therefore, even if a synoptic system originates in the south, the occurrence of Negev speleothems, and low δ^{18}O-values in the Negev, Soreq, and Dead Sea mineral precipitates, can reflect contributions from both southern and Mediterranean moisture sources.

During the peak insolation interval of MIS 5e, global sea level reached its maximum highstand, and CH_4 and CO_2 reached maximum values. At the same time, δ^{18}O in speleothems in Europe and the East Mediterranean reached their minimum values, δ^{18}O in the Greenland ice cores reached maximum values, the North Atlantic and Southern Ocean benthic foraminifera reached maximum δ^{13}C values, and European pollens of temperate trees and Mediterranean Sclerophyll reached maximum values (Govin et al., 2015). These all suggest warm and wet climate. At this time (the MIS 5e peak, 127–122 ka), we see increased precipitation in our record, with 50% of the water coming from tropical-induced rainfall, reaching three times the runoff of the modern contributions of these tropics-based climatic systems. Between 120 and 116 ka, when the Levant is characterized by a severe drought, all of the above-mentioned parameters at some point in time begin to transition away from their peak interglacial values.

While records from the north show that the wettest interval corresponds to the MIS 5e insolation peak, some records from the desert-belt appear to cover the whole MIS 5e interval. These include the Negev speleothems (Vaks et al., 2010), travertines (Waldmann et al., 2010), a paleolake in south Jordan (Petit-Maire et al., 2010) and alteration of corals to calcite due to increase in fresh water (Yehudai et al., 2017). The $^{234}U/^{238}U$ in the Dead Sea record agrees with these observations, where during the whole MIS 5e interval there are southern water sources, and provides a

quantitative context to these previous observations.

4.3. Moisture sources to the East Mediterranean

4.3.1. The MIS 5e peak

MIS 5e was characterized by intensification of the monsoon driven by peak summer insolation in the Northern Hemisphere (Prell and Kutzbach, 1987). There is evidence that this intensification, particularly over North Africa, may have affected precipitation in dry regions such as the Saharan-Arabian desert belt and even reached the Levant, causing an increase in precipitation (Rohling et al., 2002; Rosenberg et al., 2013). There is ample evidence for a wet interval in the desert belt during the monsoonal peak (Tierney et al., 2017; Vaks et al., 2010; Waldmann et al., 2010) and climate model studies confirm that the northern boundary of the African Monsoon moves north, although the models seem to show a more limited northward excursion than claimed by proxy data.

The present-day climate in the Levant is affected by tropical systems during the wet season (October to May). In particular, the intensification of the African Summer Monsoon in the Ethiopian highlands towards the late summer and fall is related to the activity of the active Red Sea Trough (ARST). This low-pressure weather system causes precipitation and flash floods in the land regions surrounding the Red Sea and into the southern Levant, usually during the fall and the spring (de Vries et al., 2013; Krichak et al., 1997). Armon et al. (2018) provide evidence that moisture from tropical regions reaches the southern Levant drylands during ARST events and in tropical plumes (TPs), which accompany the intensification of the subtropical jet stream over the region. These events are rare in the present-day climate and do not contribute a large amount of water to the Dead Sea. Precipitation and flooding in the Levant drylands is also affected by wintertime Mediterranean storms, which in some cases can reach the southern parts of the Jordan River watershed (Armon et al., 2018).

Our data and the U isotope budget show that during the peak of MIS 5e, 50% of the water came from the south and east of the watershed (from the desert belt part of the watershed). Given the estimated water runoff during that time based on Mg in the DSDDP core pore water (Kiro et al., 2017), the total flux was similar to the present-day or slightly higher (Table 3). This means that the runoff from the Jordan River decreased to almost half of its present-day flux (pre-1964), and southern runoff reached three times the present-day flux. This intensification of southern runoff may have been the result of doubling the frequency of flash floods, intensifying rainfall events and increasing precipitation in the desert belt (by both Mediterranean and tropical-induced rainfall). Doubling the precipitation in the desert belt will not have a major effect on the local climate and vegetation, but may be crucial for water resources. In addition, decreased precipitation in the Mediterranean climate zone will make it drier, but the climate will remain Mediterranean, allowing similar vegetation and formation of speleothems.

4.3.2. Moisture sources during late MIS 5e

The extreme aridity during late MIS 5e (122-116 ka) in the Levant requires a significant decrease in the activity of Mediterranean cyclones that replenish the sources of the Jordan River in the mountains at the boundary of Lebanon, Israel, and Syria, evidenced by the decrease of $^{234}U/^{238}U$ ratios of the Dead Sea from ~1.5 to ~1.0, and a relative contribution to the runoff of <10% (Section 4.1.2). This requires that precipitation must have been driven by southern climate systems that are related to the activity in the tropics. Our findings document greater aridity in the Eastern Mediterranean-Levant than the present-day during late MIS 5e, along with intense rainfall events that reached the desert belt from the south, causing precipitation and flash floods in these otherwise arid regions. Present-day storms associated with ARST synoptic systems show similar characteristics (de Vries et al., 2013), but unlike MIS 5e, they contribute a minor proportion of the moisture to the Dead Sea watershed. Combining our observations, our new Dead Sea U isotope budget (Table 3), and NCAR-CCSM3 (Otto-Bliesner et al., 2013) model simulations, we find that they corroborate each other (Section 4.4).

4.4. Comparison with climate model runs

The northern hemisphere summer climate corresponding to the MIS 5e insolation peak at ~125 ka has been simulated by climate models as part of the Paleoclimate Model Intercomparison Projects phase 3 (PMIP 3, Braconnot et al., 2012). These runs were conducted by prescribing the pertinent seasonally dependent insolation as determined by the orbital parameters, as well as the concentration of greenhouse gasses. The models respond with warming over land during boreal summers (Kutzbach et al., 2020; Lunt et al., 2013; Otto-Bliesner et al., 2013).

The 125 ka model results show higher annual precipitation than the present-day in the Levant, attributed to increased winter rainfall (Fig. 4A) and in particular due to atypically large amounts of summer rainfall (Fig. 4B). As already noted, the timing of this modeled wet interval coincides with a ~20 m long halite-free interval in the DSDDP core during the MIS 5e African wet period (127–122 ka). The model results show both the Mediterranean and the tropics as moisture sources (Kutzbach et al., 2020, 2014), consistent with the observed shift of $^{234}U/^{238}U$-values to ~1.3 (Figs. 2 and 3), and indicating increased southern moisture sources together with continued Mediterranean storm track contributions. Also, our budget for runoff to the Dead Sea (Table 3) shows ~50% of the water coming from the east and south, while the total runoff during that time is slightly higher than the present-day (Kiro et al., 2017). Combining this observation with the 125 ka climate model results indicates that this precipitation increases mainly occurred during the summer (Fig. 4B), and are related to intensification of the African Summer Monsoon over the Sahara, East Africa and Arabia.

The NCAR CCSM3 model was also run with insolation data corresponding to 120 ka and 115 ka (output from the latter run was not available to us but see Kutzbach et al., 2014, 2020). Both the DSDDP observations and these late MIS 5e CCSM3 climate simulations concur that the climate transitioned from the wetter (than present-day) interval during the insolation peak of MIS 5e at 127–122 ka to drier conditions at 122–116 ka. This transition followed a sharp decrease in summer insolation and an increase in winter insolation as the precession cycle moves towards its minimum state. The 120 ka simulation shows lower total rainfall than the present-day, through decreased winter precipitation (Fig. 4C,S6) and is thus indicating weakening of the Mediterranean moisture source that predominantly feeds present-day Levant rainfall. The timing coincides with the beginning of the extreme-drought interval, characterized by thick halite accumulation in the DSDDP-core and intervals in which the Dead Sea showed $^{234}U/^{238}U$-values of ~1.0 (Figs. 2 and 3), signaling insignificant contributions from the Jordan River. We note however that drying of the model climate at 120 ka does not appear as dramatic as indicated by the uranium isotopes. The 115 ka simulation of Kutzbach et al. (2020, 2014), when the summer insolation reaches minimum and winter simulation reaches maximum, also shows significantly drier conditions compared to the 125 ka simulation, suggesting that the dry conditions prevailed until the end of MIS 5e. During the extreme drought interval the U isotope budget (Table 2) indicates ~95% of the moisture sourced in the south, with total

runoff only ~30–50% of the present-day (Kiro et al., 2017). The runoff contribution from southern/eastern sources are ~1.5–2 times the present-day, and the Jordan River flux becomes insignificant (<10% of the present-day). As noted above, the extent of drying indicated by the DSDDP cores seems to be larger than what is seen by the 120 ka model run. This may be due to model biases or suggest that there are processes that are not considered in the model, which may have affected the amount of precipitation. For example, a recent study showed that ice melt pulses in Greenland result in decrease in precipitation over southern Europe and the Mediterranean over centennial time scales (Tzedakis et al., 2018).

The thick halite-rich interval in the core is composed of alternating halite layers that precipitated over decades to centuries, and detrital layers depositing over centuries to millennia, indicating fluctuations between extreme dry intervals with 20% of the present runoff to intervals similar to or slightly wetter than the present climate (Kiro et al., 2017).

4.5. Possible mechanisms and relevance to climate change

The cause of the severe drying of the Levant at ~122–116 ka is most-likely related to a decrease in cyclonic activity in the Mediterranean during winter, as these systems are responsible for the rainy season in the present-day climate. Consistent with this decrease in rainfall is the higher atmospheric sea level pressures over the North Atlantic, Southern Europe and the Mediterranean compared to the present-day seen in the 120 ka simulation (Fig. 6). This change in sea level pressure implies that during the late MIS 5e interval, as the precession cycle moved towards warmer winters (Fig. 7), the Atlantic storm track stayed further north of the Mediterranean and southern Europe, resulting in a weakening of the Mediterranean storm tracks. This is also consistent with a northward expansion of the subtropical subsidence over North Africa into the Mediterranean and thus an expansion of desert belt over the region (Fig. 6).

The expansion of the subtropical dry zones towards the end of MIS 5e is reminiscent of the present-day drying trend in the Eastern Mediterranean (Kelley et al., 2012) and is consistent with predictions of effects of future greenhouse gas induced climate change (D'Agostino and Lionello, 2020; Seager et al., 2014). It seems like the reduction in air-sea temperature contrast, common to the insolation minimum of 122-116 ka and the 21st century greenhouse world, are both associated with similar changes in Mediterranean winter climate.

Furthermore, the 120 ka simulation results show that while total annual precipitation decreases in the Eastern Mediterranean, there is an increase in autumn precipitation compared to today along the Red Sea, that penetrates northward towards the southern and eastern parts of the Dead Sea watershed. The increase in moisture penetration from the south, along the Red Sea, is associated with increased late-summer monsoonal activity over subtropical East Africa, including the Ethiopian Plateau (Fig. 4D) as the peak in annual insolation shifts towards late summer (Otto-Bliesner et al., 2013). At present, fall rainfall in the Eastern Mediterranean-Levant often results from ARST events (de Vries et al., 2013). The shift in the seasonal timing of precipitation towards autumn during the extreme-arid period at ~122–116 ka is consistent with increased rainfall associated with such systems. In the present-day, ARST events cause intense downpours and major flash floods in the southern Dead Sea watershed (Kahana et al., 2002). The pattern of autumn rainfall intensification at 120 ka coincides with a drift in the timing of the insolation anomaly maximum (past minus present, Fig. 5) from summer to autumn between 125–115 ka, due to change in the timing of perihelion (De Noblet et al., 1996; Otto-Bliesner et al., 2013). This shift and its effects highlight the importance of orbital forcing on subtropical synoptic systems, in this case resulting in weakened winter storms and redistribution of tropical-sourced rainfall during the warm season.

The concurrence between our MIS 5e observations and the NCAR CCSM3 simulation results lends credibility to state-of-the-art climate model predictions of global hydroclimatic changes in a warming world, including shifts in the moisture sources, intensification of rainfall events and expansion of the desert belts. In the 120 ka simulation results (Fig. 4), the source region of present-day tropical moisture incursions into the Levant by ARST systems (de Vries et al., 2013) shows heightened autumn precipitation. At the same time, climate models (Hochman et al., 2018; Peleg et al., 2015) predict decreased frequency of the Cyprus Low systems, and increased frequencies of Red Sea Trough systems, consistent with trends from modern observations (Alpert et al., 2004) and episodes that occurred during the Holocene (Ahlborn et al., 2018; Neugebauer et al., 2015). These current trends in the region, together with the observations that droughts occur along with flooding events from moisture that mainly originates from tropical systems, demonstrates an important interplay between the tropical and mid-latitude climates. Our results indicate that increased aridity in the Eastern Mediterranean-Levant may be accompanied by changes in the sources and the seasonality of moisture, and in the rainfall intensity (de Vries et al., 2013; Kahana et al., 2002). Such changes may have critical implications for water resources in the region and its socio-economic and political stability (Kelley et al., 2015).

5. Conclusions

This study documents major shifts in the geographic sources, intensity, and seasonality of Eastern Mediterranean precipitation during the last interglacial MIS 5e, reflecting global shifts in the rain and desert belts. The Eastern Mediterranean climate during MIS 5e was highly variable. The peak northern hemisphere summer insolation (127–122 ka) was relatively wet, while the late MIS 5e (122-116 ka) was extremely arid.

This scenario is based on $^{234}U/^{238}U$ activity ratios of primary (evaporitic) minerals that were deposited in the last interglacial MIS 5e Dead Sea, the lithology of the sedimentary sequences (e.g. intervals of muds versus salt deposition) combined with climate model simulations. The $^{234}U/^{238}U$ activity ratio fluctuates between ~1.5 and ~1.0. Values around 1.5 are characteristic of the water that filled the late Quaternary lakes in the Dead Sea Basin, reflecting mainly the contributions of freshwater from the Jordan River. The lower values observed at ~1.3 and ~1.0 indicate the near cessation of the Jordan River freshwater contribution to the lake and rather freshwater contributions from the southern and eastern sources of the lake's watershed.

During the insolation peak, summer tropical-induced rainfall reached the Dead Sea catchment and accounted for~50% of the total rainfall, in stark contrast to present-day dry summers, and the total rainfall was likely greater than today. This wet period was characterized by an increase in precipitation in the east and south, mainly during the summer, associated with intensification of the African monsoon, although the Mediterranean climate system was also active during that time. Following the insolation peak the region experienced an extreme drought period signified by expansion of the desert belt. The arid late MIS 5e was characterized by a major weakening of the Mediterranean storm systems feeding Jordan River sources, resulting in a major decline of its flow to ~10% of the present-day together with an increase in tropical-induced rainfall, causing an increase in southern/eastern precipitation and/or flash floods, mainly during the fall.

Author statement

Yael Kiro: Conceptualization, Methodology, Software, Validation, Formal analysis, Investigation, Writing - original draft, Visualization, Supervision, Funding acquisition; Steven L. Goldstein: Conceptualization, Resources, Writing - original draft, Supervision, Funding acquisition; Yochanan Kushnir: Conceptualization, Methodology, Software, Resources, Writing - review & editing, Supervision; Jennifer M. Olson: Investigation; Louise Bolge: Methodology, Resources; Boaz Lazar: Funding acquisition; Mordechai Stein: Validation, Writing - review & editing, Funding acquisition.

Declaration of competing interest

The authors declare that they have no known competing financial interests or personal relationships that could have appeared to influence the work reported in this paper.

Acknowledgments

We thank Bette Otto-Bliesner, John Kutzbach, and Efrat Morin for discussions. We thank Adi Torfstein for trace element data. This study was supported by the US NSF (Grant EAR-1635391 to YK, SLG and YK), the US-Israel Binational Science Foundation (USIBSF, Grant #2010375 to SLG and MS), the Dead Sea Drill Excellence Center of the Israel Science Foundation (grant #1736/11 to BL), the Climate Center of Lamont-Doherty Earth Observatory, and the Storke Endowment of the Department of Earth and Environmental Sciences of Columbia University. Drilling for the Dead Sea Deep Drill Core was partly supported by NSF grant EAR 11–15312. Jennifer Olson was a Research Experiences for Undergraduates student, supported by the LDEO NSF REU Grant OCE-1359194. Y. Kushnir also acknowledges support from NSF award AGS-1734760. This is Dead Sea Excellence Center contribution #37 and LDEO contribution #8440.

Appendix A. Supplementary data

Supplementary data to this article can be found online at https://doi.org/10.1016/j.quascirev.2020.106546.

References

Ahlborn, M., Armon, M., Ben Dor, Y., Neugebauer, I., Schwab, M.J., Tjallingii, R., Shoqeir, J.H., Morin, E., Enzel, Y., Brauer, A., 2018. Increased frequency of torrential rainstorms during a regional late Holocene eastern Mediterranean drought. Quat. Res. (United States) 89, 425–431. https://doi.org/10.1017/qua.2018.9.

Alpert, P., 2002. The paradoxical increase of Mediterranean extreme daily rainfall in spite of decrease in total values. Geophys. Res. Lett. 29 (1536) https://doi.org/10.1029/2001GL013554.

Alpert, P., Osetinsky, I., Ziv, B., Shafir, H., 2004. Semi-objective classification for daily synoptic systems: application to the Eastern Mediterranean climate change. Int. J. Climatol. 24, 1001–1011. https://doi.org/10.1002/joc.1036.

Armon, M., Dente, E., Smith, J.A., Enzel, Y., Morin, E., 2018. Synoptic-scale control over modern rainfall and flood patterns in the levant drylands with implications for past climates. J. Hydrometeorol. 19, 1077–1096. https://doi.org/10.1175/JHM-D-18-0013.1.

Bar-Matthews, M., 2014. History of Water in the Middle East and North Africa. In: Holland, H., Turekian, K. (Eds.), Treatise on Geochemistry. Elsevier, pp. 109–128. https://doi.org/10.1016/B978-0-08-095975-7.01210-9.

Bar-Matthews, M., Ayalon, A., Gilmour, M., Matthews, A., Hawkesworth, C.J., 2003. Sea – land oxygen isotopic relationships from planktonic foraminifera and speleothems in the Eastern Mediterranean region and their implication for paleorainfall during interglacial intervals. Geochem. Cosmochim. Acta 67, 3181–3199.

Bartov, Y., Goldstein, S.L., Stein, M., Enzel, Y., 2003. Catastrophic arid episodes in the eastern mediterranean linked with the north Atlantic heinrich events. Geology 31, 439–442. https://doi.org/10.1130/0091-7613(2003)031<0439.

Bartov, Y., Stein, M., Enzel, Y., Agnon, A., Reches, Z., 2002. Lake Levels and Sequence Stratigraphy of Lake Lisan, the Late Pleistocene Precursor of the Dead Sea. Quat. Res. 57, 9–21. https://doi.org/10.1006/qres.2001.2284.

Battisti, D.S., Ding, Q., Roe, G.H., 2014. Coherent pan-Asian climatic and isotopic response to orbital forcing of tropical insolation. J. Geophys. Res. Atmos. 119, 11997–12020. https://doi.org/10.1002/2014JD021960.Received.

Bereiter, B., Eggleston, S., Schmitt, J., Nehrbass-Ahles, C., Stocker, T.F., Fischer, H., Kipfstuhl, S., Chappellaz, J., 2015. Antarctic ice cores revised 800KYr CO2 data. http://ncdc.noaa.gov/paleo/study/17975.

Bosmans, J.H.C., van der Ent, R.J., Haarsma, R.J., Drijfhout, S.S., Hilgen, F.J., 2020. Precession- and obliquity-induced changes in moisture sources for enhanced precipitation over the mediterranean sea. Paleoceanogr. Paleoclimatol. 35, 1–14. https://doi.org/10.1029/2019PA003655.

Braconnot, P., Harrison, S.P., Kageyama, M., Bartlein, P.J., Masson-Delmotte, V., Abe-Ouchi, A., Otto-Bliesner, B., Zhao, Y., 2012. Evaluation of climate models using palaeoclimatic data. Nat. Clim. Change 2, 417–424. https://doi.org/10.1038/nclimate1456.

Brauer, A., Allen, J.R.M., Mingram, J., Dulski, P., Wulf, S., Huntley, B., 2007. Evidence for last interglacial chronology and environmental change from Southern Europe. Proc. Natl. Acad. Sci. 104, 450–455. https://doi.org/10.1073/pnas.0603321104.

Collins, M., Knutti, R., Arblaster, J., Dufresne, J.-L., Fichefet, T., Friedlingstein, P., Gao, X., Gutowski, W.J., Johns, T., Krinner, G., Shongwe, M., Tebaldi, C., Weaver, A.J., Wehner, M., 2013. Long-term climate change: projections, commitments and irreversibility. In: Stocker, T.F., Qin, D., Plattner, G.-K., Tignor, M., Allen, S.K., Boschung, J., Nauels, A., Xia, Y., Bex, V., Midgley, P.M. (Eds.), Climate Change 2013: the Physical Science Basis. Contribution of Working Group I to the Fifth Assessment Report of the Intergovernmental Panel on Climate Change. Cambridge University Press, NY, USA, pp. 1029–1136. https://doi.org/10.1017/CBO9781107415324.024. Cambridge, United Kingdom and New York.

D'Agostino, R., Lionello, P., 2020. The atmospheric moisture budget in the Mediterranean: mechanisms for seasonal changes in the Last Glacial Maximum and future warming scenario. Quat. Sci. Rev. 241 (106392) https://doi.org/10.1016/j.quascirev.2020.106392.

De Noblet, N., Braconnot, P., Joussaume, S., Masson, V., 1996. Sensitivity of simulated Asian and African summer monsoons to orbitally induced variations in insolation 126, 115 and 6 kBP. Clim. Dynam. 12, 589–603. https://doi.org/10.1007/BF00216268.

de Vries, A.J., Tyrlis, E., Edry, D., Krichak, S.O., Steil, B., Lelieveld, J., 2013. Extreme precipitation events in the Middle East: dynamics of the active Red Sea trough. J. Geophys. Res. Atmos. 118, 7087–7108. https://doi.org/10.1002/jgrd.50569.

Develle, A.-L., Gasse, F., Vidal, L., Williamson, D., Demory, F., Van Campo, E., Ghaleb, B., Thouveny, N., 2011. A 250ka sedimentary record from a small karstic lake in the Northern Levant (Yammoûneh, Lebanon). Palaeogeogr. Palaeoclimatol. Palaeoecol. 305, 10–27. https://doi.org/10.1016/j.palaeo.2011.02.008.

Donat, M.G., Angélil, O., Ukkola, A.M., 2019. Intensification of precipitation extremes in the world's humid and water- limited regions. Environ. Res. Lett. 14, 1–9.

Douady, C.J., Catzeflis, F., Raman, J., Springer, M.S., Stanhope, M.J., 2003. The Sahara as a vicariant agent, and the role of Miocene climatic events, in the diversification of the mammalian order Macroscelidea (elephant shrews). Proc. Natl. Acad. Sci. Unit. States Am. 100, 8325–8330. https://doi.org/10.1073/pnas.0832467100.

Drake, N.A., Blench, R.M., Armitage, S.J., Bristow, C.S., White, K.H., 2011. Ancient watercourses and biogeography of the Sahara explain the peopling of the desert. Proc. Natl. Acad. Sci. Unit. States Am. 108, 458–462. https://doi.org/10.1073/pnas.1012231108.

Dutton, A., Lambeck, K., 2012. Ice volume and sea level during the last interglacial. Science 337, 216–219.

Enzel, Y., Bookman Ken-Tor, R., Sharon, D., Gvirtzman, H., Dayab, U., Ziv, B., Stein, M., 2003. Late Holocene climates of the Near East deduced from Dead Sea level variations and modern regional winter rainfall. Quat. Res. 60, 263–273. https://doi.org/10.1016/j.yqres.2003.07.011.

Felis, T., Lohmann, G., Kuhnert, H., Lorenz, S.J., Scholz, D., Pätzold, J., Al-Rousan, S.A., Al-Moghrabi, S.M., 2004. Increased seasonality in Middle East temperatures during the last interglacial period. Nature 429, 164–168. https://doi.org/10.1038/nature02546.

Fick, S.E., Hijmans, R.J., 2017. WorldClim 2: new 1-km spatial resolution climate surfaces for global land areas. Int. J. Climatol. https://doi.org/10.1002/joc.5086.

Frumkin, A., Stein, M., 2004. The Sahara-East Mediterranean dust and climate connection revealed by strontium and uranium isotopes in a Jerusalem speleothem. Earth Planet Sci. Lett. 217, 451–464. https://doi.org/10.1016/S0012-821X(03)00589-2.

Gat, J.R., Carmi, I., 1987. Effect of climate changes on the precipitation patterns and isotopic composition of water in a climate transition zone: case of the eastern mediterranean sea area, in: the influence of climate change and climatic variablity on hydrologic regime and water resources (proceedings of the vancouver symposium). IAHS publ.., pp. 513–524

Goldstein, S.L., Kiro, Y., Torfstein, A., Kitagawa, H., Tierney, J.E., Stein, M., 2020. Revised chronology of the ICDP Dead Sea deep drill core relates drier-wetter-drier climate cycles to insolation over the past 220 kyr. Quat. Sci. Rev. this volume.

Govin, A., Capron, E., Tzedakis, P.C., Verheyden, S., Ghaleb, B., Hillaire-Marcel, C., St-Onge, G., Stoner, J.S., Bassinot, F., Bazin, L., Blunier, T., Combourieu-Nebout, N., El Ouahabi, A., Genty, D., Gersonde, R., Jimenez-Amat, P., Landais, A., Martrat, B., Masson-Delmotte, V., Parrenin, F., Seidenkrantz, M.-S., Veres, D., Waelbroeck, C., Zahn, R., 2015. Sequence of events from the onset to the demise of the Last

Interglacial: evaluating strengths and limitations of chronologies used in climatic archives. Quat. Sci. Rev. 129, 1–36. https://doi.org/10.1016/j.quascirev.2015.09.018.
Grant, K.M., Grimm, R., Mikolajewicz, U., Marino, G., Ziegler, M., Rohling, E.J., 2016. The timing of Mediterranean sapropel deposition relative to insolation, sea-level and African monsoon changes. Quat. Sci. Rev. 140, 125–141. https://doi.org/10.1016/j.quascirev.2016.03.026.
Grant, K.M., Rohling, E.J., Bar-Matthews, M., Ayalon, a., Medina-Elizalde, M., Ramsey, C.B., Satow, C., Roberts, a. P., 2012. Rapid coupling between ice volume and polar temperature over the past 150,000 years. Nature 491, 744–747. https://doi.org/10.1038/nature11593.
Haase-Schramm, A., Goldstein, S.L., Stein, M., 2004. U-Th dating of Lake Lisan (late Pleistocene Dead Sea) aragonite and implications for glacial East Mediterranean climate change. Geochem. Cosmochim. Acta 68, 985–1005. https://doi.org/10.1016/j.gca.2003.07.016.
Hall, J.K., 1997. Topography and bathymetry of the Dead Sea depression. In: Niemi, T.M., Ben-Avraham, Z., Gat, J.R. (Eds.), The Dead Sea – the Lake and its Settings. Oxford Monographs on Geology and Geophysics No. 36, pp. 11–21.
Held, I.M., Soden, B.J., 2006. Robust responses of the hydrological cycle to global warming. J. Clim. 19, 5686–5699.
Hellstrom, J.C., McCulloch, M.T., 2000. Multi-proxy constraints on the climatic significance of trace element records from a New Zealand speleothem. Earth Planet Sci. Lett. 179, 287–297. https://doi.org/10.1016/S0012-821X(00)00115-1.
Hochman, A., Harpaz, T., Saaroni, H., Alpert, P., 2018. Synoptic classification in 21st century CMIP5 predictions over the Eastern Mediterranean with focus on cyclones. Int. J. Climatol. 38, 1476–1483. https://doi.org/10.1002/joc.5260.
Jouzel, J., Masson-Delmotte, V., Cattani, O., Dreyfus, G., Falourd, S., Hoffmann, G., Minster, B., Nouet, J., Barnola, J.M., Chappellaz, J., Fischer, H., Gallet, J.C., Johnsen, S., Leuenberger, M., Loulergue, L., Luethi, D., Oerter, H., Parrenin, F., Raisbeck, G., Raynaud, D., Schilt, a, Schwander, J., Selmo, E., Souchez, R., Spahni, R., Stauffer, B., Steffensen, J.P., Stenni, B., Stocker, T.F., Tison, J.L., Werner, M., Wolff, E.W., 2007. Orbital and millennial Antarctic climate variability over the past 800,000 years. Science 317, 793–796. https://doi.org/10.1126/science.1141038.
Kahana, R., Ziv, B., Enzel, Y., Dayan, U., 2002. Synoptic climatology of major floods in the Negev Desert. Israel. Int. J. Climatol 22, 867–882. https://doi.org/10.1002/joc.766.
Kaniewski, D., Van Campo, E., Weiss, H., 2012. Drought is a recurring challenge in the Middle East. Proc. Natl. Acad. Sci. U. S. A. 109, 3862–3867. https://doi.org/10.1073/pnas.1116304109.
Katz, A., Starinsky, A., 2008. Geochemical history of the Dead Sea. Aquat. Geochemistry 15, 159–194. https://doi.org/10.1007/s10498-008-9045-0.
Kaufman, A., Wasserburg, G.J., Porcelli, D., Bar-Matthews, M., Ayalon, A., Halicz, L., 1998. U-Th isotope systematics from the Soreq cave, Israel and climatic correlations. Earth Planet Sci. Lett. 156, 141–155. https://doi.org/10.1016/S0012-821X(98)00002-8.
Kelley, C., Ting, M., Seager, R., Kushnir, Y., 2012. The relative contributions of radiative forcing and internal climate variability to the late 20th Century winter drying of the Mediterranean region. Clim. Dyn. 38, 2001–2015. https://doi.org/10.1007/s00382-011-1221-z.
Kelley, C.P., Mohtadi, S., Cane, M.A., Seager, R., Kushnir, Y., 2015. Climate change in the Fertile Crescent and implications of the recent Syrian drought. Proc. Natl. Acad. Sci. Unit. States Am. 112, 3241–3246. https://doi.org/10.1073/pnas.1421533112.
Kiro, Y., Goldstein, S.L., García-Veigas, J., Levy, E., Kushnir, Y., Stein, M., Lazar, B., 2017. Relationships between lake level changes and water and salt budgets in the Dead Sea during extreme aridities in the Eastern Mediterranean. Earth Planet Sci. Lett. 464, 211–226. https://doi.org/10.1016/j.epsl.2017.01.043.
Kiro, Y., Goldstein, S.L., Lazar, B., Stein, M., 2016. Environmental implications of salt facies in the Dead Sea. Geol. Soc. Am. Bull. 128, 824–841. https://doi.org/10.1130/B31357.1.
Kiro, Y., Weinstein, Y., Starinsky, A., Yechieli, Y., 2015. Application of radon and radium isotopes to groundwater flow dynamics: An example from the Dead Sea. Chem. Geol. 411, 155–171. https://doi.org/10.1016/j.chemgeo.2015.06.014.
Kiro, Y., Weinstein, Y., Starinsky, A., Yechieli, Y., 2014. The extent of seawater circulation in the aquifer and its role in elemental mass balances: a lesson from the Dead Sea. Earth Planet Sci. Lett. 394, 146–158. https://doi.org/10.1016/j.epsl.2014.03.010.
Kolodny, Y., Stein, M., Machlus, M., 2005. Sea-rain-lake relation in the last glacial East Mediterranean revealed by δ18O-δ13C in lake lisan aragonites. Geochem. Cosmochim. Acta 69, 4045–4060. https://doi.org/10.1016/j.gca.2004.11.022.
Krichak, S.O., Alpert, P., Krishnamurti, T.N., 1997. Red Sea trough/cyclone development- numerical investigation. Meterology Atmos. Phys. 169, 159–169.
Kronfeld, J., Ilani, S., Strull, A., 1991. Radium precipitation and extreme 238U-series disequilibrium along the Dead Sea coast. Israel. Appl. Geochem. 6, 355–361.
Ku, T., Knauss, K.G., Mathieu, G.G., 1977. Uranium in open ocean: concentration and isotopic composition. Deap-Sea Res. 24, 1005–1017.
Kushnir, Y., Stein, M., 2010. North Atlantic influence on 19th–20th century rainfall in the Dead Sea watershed, teleconnections with the Sahel, and implication for Holocene climate fluctuations. Quat. Sci. Rev. 29, 3843–3860. https://doi.org/10.1016/j.quascirev.2010.09.004.
Kutzbach, J.E., Chen, G., Cheng, H., Edwards, R.L., Liu, Z., 2014. Potential role of winter rainfall in explaining increased moisture in the Mediterranean and Middle East during periods of maximum orbitally-forced insolation seasonality. Clim. Dynam. 42, 1079–1095. https://doi.org/10.1007/s00382-013-1692-1.
Kutzbach, J.E., Guan, J., He, F., Cohen, A.S., Orland, I.J., Chen, G., 2020. African climate response to orbital and glacial forcing in 140,000-y simulation with implications for early modern human environments. Proc. Natl. Acad. Sci. U. S. A. 117, 2255–2264. https://doi.org/10.1073/pnas.1917673117.
Lahr, M.M., Foley, R., 1994. Multiple dispersals and modern human origins. Evol. Anthropol. 3, 48–60. https://doi.org/10.1002/evan.1360030206.
Laskar, J., Robutel, P., Joutel, F., Gastineau, M., Correia, A.C.M., Levrard, B., 2004. A long-term numerical solution for the insolation quantities of the Earth. Astron. Astrophys. Nor. 428, 261–285. https://doi.org/10.1051/0004-6361:20041335.
Lensky, N.G., Dvorkin, Y., Lyakhovsky, V., Gertman, I., Gavrieli, I., 2005. Water, salt, and energy balances of the Dead Sea. Water resour. Res. 41, W12418. https://doi.org/10.1029/2005WR004084.
Levy, E.J., Stein, M., Lazar, B., Yechieli, Y., Gavrieli, I., Sivan, O., 2016. Pore fluids in Dead Sea sediment core reveal linear response of lake chemistry to global climate changes. Geology G38685.1. https://doi.org/10.1130/G38685.1.
Lisiecki, L.E., Raymo, M.E., 2005. A Pliocene-Pleistocene stack of 57 globally distributed benthic δ 18 O records. Paleoceanography 20, 1–17. https://doi.org/10.1029/2004PA001071.
Lunt, D.J., Abe-Ouchi, A., Bakker, P., Berger, A., Braconnot, P., Charbit, S., Fischer, N., Herold, N., Jungclaus, J.H., Kohn, V., Krebs-Kanzow, U., Lohmann, G., Otto-Bliesner, B., Park, W., Pfeiffer, M., Prange, M., Rachmayani, R., Renssen, H., Rosenbloom, N., Schneider, B., Stone, E.J., Takahashi, K., Wei, W., Yin, Q., 2013. A multi-model assessment of last interglacial temperatures. Clim. Past 9, 699–717. https://doi.org/10.5194/cp-9-699-2013. <https://doi.org/10.5194/cp-9-699-2013>, hdl:10013/epic.41201.
Lüthi, D., Le Floch, M., Bereiter, B., Blunier, T., Barnola, J.-M., Siegenthaler, U., Raynaud, D., Jouzel, J., Fischer, H., Kawamura, K., Stocker, T.F., 2008. High-resolution carbon dioxide concentration record 650,000–800,000 years before present. Nature 453, 379–382. https://doi.org/10.1038/nature06949.
McGarry, S., Bar-Matthews, M., Matthews, A., Vaks, A., Schilman, B., Ayalon, A., 2004. Constraints on hydrological and paleotemperature variations in the Eastern Mediterranean region in the last 140ka given by the δD values of speleothem fluid inclusions. Quat. Sci. Rev. 23, 919–934. https://doi.org/10.1016/j.quascirev.2003.06.020.
Molnar, P., 2001. Climate change, flooding in arid environments, and erosion rates. Geology 29, 1071–1074. https://doi.org/10.1130/0091-7613(2001)029<1071:CCFIAE>2.0.CO.
Neev, D., Emery, K.O., 1967. The Dead Sea: depositional process and environments of evaporites. Geol. Surv. Isr. Bull. 41, 147.
Nehme, C., Verheyden, S., Noble, S.R., Farrant, A.R., Sahy, D., Hellstrom, J., Delannoy, J.J., Claeys, P., 2015. Reconstruction of MIS 5 climate in the central Levant using a stalagmite from Kanaan Cave, Lebanon. Clim. Past 11, 1785–1799. https://doi.org/10.5194/cp-11-1785-2015.
Neugebauer, I., Brauer, A., Schwab, M.J., Dulski, P., Frank, U., Hadzhiivanova, E., Kitagawa, H., Litt, T., Schiebel, V., Taha, N., Waldmann, N.D., Party, D.S., 2015. Evidences for centennial dry periods at ~3300 and ~2800 cal. yr BP from micro-facies analyses of the Dead Sea sediments. Holocene 25, 1358–1371. https://doi.org/10.1177/0959683615584208.
Neugebauer, I., Brauer, A., Schwab, M.J., Waldmann, N.D., Enzel, Y., Kitagawa, H., Torfstein, A., Frank, U., Dulski, P., Agnon, A., Ariztegui, D., Ben-Avraham, Z., Goldstein, S.L., Stein, M., 2014. Lithology of the long sediment record recovered by the ICDP Dead Sea deep drilling Project (DSDDP). Quat. Sci. Rev. 102, 149–165. https://doi.org/10.1016/j.quascirev.2014.08.013.
Neugebauer, I., Schwab, M.J., Waldmann, N.D., Tjallingii, R., Frank, U., Hadzhiivanova, E., Naumann, R., Taha, N., Agnon, A., Enzel, Y., Brauer, A., 2016. Hydroclimatic variability in the Levant during the early last glacial (~117–75 ka) derived from micro-facies analyses of deep Dead Sea sediments. Clim. Past 12, 75–90. https://doi.org/10.5194/cpd-11-3625-2015.
Nicholson, S.L., Pike, A.W.G., Hosfield, R., Roberts, N., Sahy, D., Woodhead, J., Cheng, H., Edwards, R.L., Affolter, S., Leuenberger, M., Burns, S.J., Matter, A., Fleitmann, D., 2020. Pluvial periods in Southern Arabia over the last 1.1 million-years. Quat. Sci. Rev. 229 (106112) https://doi.org/10.1016/j.quascirev.2019.106112.
Orland, I.J., He, F., Bar-Matthews, M., Chen, G., Ayalon, A., Kutzbach, J.E., 2019. Resolving seasonal rainfall changes in the Middle East during the last interglacial period. Proc. Natl. Acad. Sci. U. S. A. 116, 24985–24990. https://doi.org/10.1073/pnas.1903139116.
Osborne, A.H., Vance, D., Rohling, E.J., Barton, N., Rogerson, M., Fello, N., 2008. A humid corridor across the Sahara for the migration of early modern humans out of Africa 120,000 years ago. Proc. Natl. Acad. Sci. Unit. States Am. 105, 16444–16447. https://doi.org/10.1073/pnas.0804472105.
Otto-Bliesner, B.L., Rosenbloom, N., Stone, E.J., Mckay, N.P., Lunt, D.J., Brady, E.C., Overpeck, J.T., 2013. How warm was the last interglacial? New model – data comparisons. Philos. Trans. R. Soc. A 371, 1–20.
Paillard, D., Labeyrie, L., Yiou, P., 1996. Macintosh Program performs time-series analysis. Eos. Trans. Am. Geophys. Union 77. https://doi.org/10.1029/96EO00259, 379–379.
Peleg, N., Bartov, M., Morin, E., 2015. CMIP5-predicted climate shifts over the East Mediterranean: implications for the transition region between Mediterranean and semi-arid climates. Int. J. Climatol. 35, 2144–2153. https://doi.org/10.1002/joc.4114.
Petit-Maire, N., Carbonel, P., Reyss, J.L., Sanlaville, P., Abed, A., Bourrouilh, R., Fontugne, M., Yasin, S., 2010. A vast Eemian palaeolake in Southern Jordan (29 ° N). Glob. Planet. Change 72, 368–373. https://doi.org/10.1016/

j.gloplacha.2010.01.012.
Porcelli, D., Swarzenski, P.W., 2003. The Behavior of U- and Th-Series Nuclides in Groundwater. In: Bourdon, B., Henderson, G.M., Lundstorm, C.C., Turner, S.P. (Eds.), Uranium-Series Geochemistry. Miineralogical society of America, Washington, pp. 317–361.
Prell, W.L., Kutzbach, J.E., 1987. Monsoon variability over the past 150,000 years. J. Geophys. Res. 92, 8411–8425.
Ramsey, C.B., Plicht, J. van der, Weninger, B, 2001. "Wiggle Matching" Radiocarbon Dates. Radiocarbon 43 (2), 381–389.
Robinson, L.F., Henderson, G.M., Hall, L., Matthews, I., 2004. Climatic control of riverine and seawater uranium-isotope ratios. Science 305, 851–854. https://doi.org/10.1126/science.1099673.
Rohling, E.J., Cane, T.R., Cooke, S., Sprovieri, M., Bouloubassi, I., Emeis, K.C., Schiebel, R., Kroon, D., Jorissen, F.J., Lorre, a., Kemp, a, E.S, 2002. African monsoon variability during the previous interglacial maximum. Earth Planet Sci. Lett. 202, 61–75. https://doi.org/10.1016/S0012-821X(02)00775-6.
Rosenberg, T.M., Preusser, F., Risberg, J., Plikk, A., Kadi, K.A., Matter, A., Fleitmann, D., 2013. Middle and Late Pleistocene humid periods recorded in palaeolake deposits of the Nafud desert, Saudi Arabia. Quat. Sci. Rev. 70, 109–123. https://doi.org/10.1016/j.quascirev.2013.03.017.
Rossignol-Strick, M., 1983. African monsoons, an immediate climate response to orbital insolation. Nature 304, 46–49. https://doi.org/10.1038/304046a0.
Salameh, E., 1996. Water Quality Degradation in Jordan (Impacts on Environment, Economy and Future Generations Resources Base). Royal Society for the Conservation of Nature and Friedrich-Ebert-Stiftung. Jordan, Amman.
Salameh, E., El-Naser, H., 1999. Does the actual drop in Dead Sea level reflect the development of water sources within its drainage basin? Acta Hydrochim. Hydrobiol. (Sofia) 27, 5–11.
Salameh, E., Udluft, P., 1985. A hydrodynamic model for central Jordan. Geol. Jahrb. 38, 39–53.
Seager, R., Liu, H., Henderson, N., Simpson, I., Kelley, C., Shaw, T., Kushnir, Y., Ting, M., 2014. Causes of increasing Aridification of the mediterranean region in response to rising greenhouse gases. J. Clim. 27, 4655–4676. https://doi.org/10.1175/JCLI-D-13-00446.1.
Shackleton, N.J., 1969. The last interglacial in the marine and terrestrial records. Proc. Res. Soc. B Biol. Sci. 174, 135–154. https://doi.org/10.1098/rspb.1969.0085.
Shackleton, N.J., Sánchez-Goñi, M.F., Pailler, D., Lancelot, Y., 2003. Marine isotope substage 5e and the Eemian interglacial. Global Planet. Change 36, 151–155. https://doi.org/10.1016/S0921-8181(02)00181-9.
Stanhill, G., 1994. Changes in the rate of evaporation from the Dead Sea. Int. J. Climatol. 14, 465–471.
Tierney, J.E., Peter, B., Zander, P.D., 2017. A climatic context for the out-of-Africa migration. Geology 45, 1023–1026. https://doi.org/10.1130/G39457.1.
Torfstein, A., Goldstein, S.L., Kagan, E.J., Stein, M., 2013. Integrated multi-site U-Th chronology of the lst glacial Lake Lisan. Geochem. Cosmochim. Acta 104, 210–231.
Torfstein, A., Goldstein, S.L., Kushnir, Y., Enzel, Y., Haug, G., Stein, M., 2015. Dead Sea drawdown and monsoonal impacts in the Levant during the last interglacial. Earth Planet Sci. Lett. 412, 235–244.
Torfstein, A., Haase-Schramm, A., Waldmann, N., Kolodny, Y., Stein, M., 2009. U-series and oxygen isotope chronology of the mid-Pleistocene Lake Amora (Dead Sea basin). Geochem. Cosmochim. Acta 73, 2603–2630. https://doi.org/10.1016/j.gca.2009.02.010.
Tzedakis, P.C., Drysdale, R.N., Margari, V., Skinner, L.C., Meniviel, L., Rhodes, R.H., Taschetto, A.S., Hodell, D.A., Crowhurst, S.J., Hellstrom, J.C., Fallick, A.E., Grimalt, J.O., Mcmanus, J.F., Martrat, B., Mokeddem, Z., Parrenin, F., Regattieri, E., Roe, K., Zanchetta, G., 2018. Enhanced climate instability in the north Atlantic and southern Europe during the last interglacial. Nat. Commun. In press. https://doi.org/10.1038/s41467-018-06683-3.
Vaks, A., Bar-Matthews, M., Ayalon, A., Matthews, A., Frumkin, A., Dayan, U., Halicz, L., Almogi-Labin, A., Schilman, B., 2006. Paleoclimate and location of the border between Mediterranean climate region and the Saharo–Arabian Desert as revealed by speleothems from the northern Negev Desert. Israel. Earth Planet. Sci. Lett. 249, 384–399. https://doi.org/10.1016/j.epsl.2006.07.009.
Vaks, A., Bar-Matthews, M., Matthews, A., Ayalon, A., Frumkin, A., 2010. Middle-late quaternary paleoclimate of northern margins of the saharan-Arabian desert: reconstruction from speleothems of Negev desert. Israel. Quat. Sci. Rev. 29, 2647–2662. https://doi.org/10.1016/j.quascirev.2010.06.014.
Waldmann, N., Stein, M., Ariztegui, D., Starinsky, A., 2009. Stratigraphy, depositional environments and level reconstruction of the last interglacial Lake Samra in the Dead Sea basin. Quat. Res. 72, 1–15. https://doi.org/10.1016/j.yqres.2009.03.005.
Waldmann, N., Torfstein, A., Stein, M., 2010. Northward intrusions of low- and mid-latitude storms across the Saharo-Arabian belt during past interglacials. Geology 38, 567–570. https://doi.org/10.1130/G30654.1.
Wang, P., Tian, J., Lourens, L.J., 2010. Obscuring of long eccentricity cyclicity in Pleistocene oceanic carbon isotope records. Earth Planet Sci. Lett. 290, 319–330. https://doi.org/10.1016/j.epsl.2009.12.028.
Yehudai, M., Lazar, B., Bar, N., Kiro, Y., Agnon, A., Shaked, Y., Stein, M., 2017. U–Th dating of calcite corals from the Gulf of Aqaba. Geochim. Cosmochim. Acta 198. https://doi.org/10.1016/j.gca.2016.11.005.